rijksuniversiteit groningen

Bachelor Integration Project

Modeling and Simulation of Frequency Dynamics in Inverter-Based Microgrids

Student	Thijs de Vries (s4948238)
Programme	Industrial Engineering and Management (IEM)
Faculty	Faculty of Science and Engineering
Research Group	DTPA
Supervisor(s)	Prof. dr. Michele Cucuzzella, Xinjiang Cai
Date	February 2, 2026

Bachelor Integration Project Faculty of Science and Engineering
University of Groningen
The Netherlands

Abstract

With the increasing penetration of renewable energy sources, the natural inertia traditionally provided by synchronous generators has significantly decreased. Hence, maintaining stable frequency dynamics in power grids has become a challenge. This project investigates and compares the frequency behavior of the three grid-forming control strategies: traditional Droop Control and Virtual Synchronous Machine (VSM), and the newly emerging Matching Control.

A detailed Simulink model of an islanded microgrid with two inverters is developed, including realistic transmission lines and LCL filters. Each control strategy is implemented in this exact model to ensure a fair comparison under identical operating conditions. At $t = 0.1\,\mathrm{s}$ a load increase is introduced. The system frequency is measured using a phase-locked loop (PLL) synchronized to the three-phase point of common coupling (PCC) voltage V0abc. Using this measurement, the system response is analyzed based on frequency, active and reactive power, RMS voltage regulation, and voltage and current waveforms in the abc reference frame.

The simulation results show that Droop Control and VSM Control have similar frequency responses characterized by oscillatory transient behavior and steady-state frequency deviation. Matching Control shows a very different dynamic behavior, with reduced oscillations and smoother power response. However, the dip in frequency is slightly deeper. The results emphasize the trade-offs between simplicity and dynamic performance, and provide insights into the suitability of each control strategy in inverter-based microgrids.

Contents

1 Introduction

The stability of electric power grids is closely related to the system's frequency dynamics. In traditional grids, the frequency is controlled by the inertia of synchronous generators. These generators naturally resist sudden changes in power supply and demand [1]. However, with the implementation of more renewable energy sources and the transition to inverter-based microgrids, this natural inertia decreases, making frequency regulation more challenging [2]. To maintain reliability in low-inertia systems, understanding and accurately modeling frequency dynamics is crucial.

Recent research has proposed several control strategies to address the lack of inertia in inverter-based microgrids. Droop Control and Virtual Synchronous Machine (VSM) / Virtual Synchronous Generator (VSG) are widely studied, as they imitate the behavior of traditional synchronous machines [3]. Although these methods have proven to be effective in simulations and pilot projects, questions remain about their accuracy, scalability, and reliability under various grid conditions [4, 5].

This thesis makes the following contributions:

- Simulation model: Development of a detailed MATLAB/Simulink model of an islanded inverter-based microgrid with two grid-forming inverters, including LCL filters, transmission lines, and realistic load dynamics.
- Controller implementation: Implementation of three grid-forming control strategies; Droop Control, VSM control, and Matching Control in the same model to ensure a fair comparison.
- KPI-based evaluation: Comparison of the control strategies based on key performance indicators (KPIs), including frequency response, active and reactive power dynamics, RMS voltage regulation, and voltage and current waveforms in the abc reference frame.

The remainder of this report is organized as follows. Section 2 presents the problem statement. Section 3 analyzes the problem and identifies the relevant stakeholders. The recommendations of enserink et al. [6] are followed to provide a detailed system description. A stakeholder analysis will be conducted to identify the key actors and classify them according to their roles and interests in the problem [7]. The system description elaborates on the system that needs to be controlled. In Section 4, the research questions will be stated. Section 5 elaborates on the knowledge gap and introduces the key concepts of inverter-based frequency control. Section 6 focuses on the economic impact and industrial relevance of stable frequency operation. The methods and materials used will be discussed in Section 7. An overview of the used control strategies will be given in Section 8. Section 9 presents the Simulink model used and how it was built. In Section 10, the results of the three control strategies will be analyzed based on selected parameters. In Section 11, the results of the control strategies will be compared. The report concludes with a conclusion in Section 12.

2 Problem Statement

Grid-forming control strategies such as Droop Control, VSM Control, and Matching Control are mostly studied in theoretical or simplified contexts, while simulation-based validation is limited. Hence, their ability to reproduce realistic frequency, voltage, and power dynamics under disturbances in inverter-based microgrids remains insufficiently tested.

3 Problem Analysis

3.1 System Description

The system under study is an islanded microgrid, a system built to function independently without the transmission of power to the main power grid. The generation in this islanded microgrid is dominated by inverter-based distributed energy resources (DERs), including photovoltaic (PV) panels, battery energy storage systems, and wind turbines. These DERs are linked together by grid-forming inverters that use either Droop Control or VSM to regulate frequency and power distribution.

The primary focus in the system is to what extent the control methods can stabilize the system's frequency in the presence of disturbances, such as load steps or fluctuations in electricity generation. The inverters and the control methods should ensure that power supply and demand stay balanced, even in the absence of synchronous machines with their natural inertia. The analysis also considers a frequency measurement and control loop, which represents the feedback mechanism that detects deviations from the nominal frequency and adjusts inverter output accordingly.

The transmission grid is excluded since the focus is on the islanded operation. Similarly, secondary frequency control, market mechanisms, and communication networks are not included in the model. Additionally, external influences such as weather and compliance with standards or grid codes are acknowledged but not modeled.

By focusing the system on DERs, inverters, loads, and primary control systems, the research captures the short time-scale behavior that is most crucial for the stability and reliability of inverter-based microgrids. This provides a clear comparison between Droop and VSM Control strategies, focusing on their frequency stability and real-world performance.

3.2 Problem Owner

The Department of Discrete Technology and Production Automation (DTPA), Faculty of Science and Engineering, University of Groningen (RUG), is the problem owner in this study. Prof. Michele Cucuzzella, the supervisor, represents the research group which is interested in the modeling and frequency dynamics of inverter-based microgrids.

The DTPA research team will be the main beneficiary of the knowledge produced, but academic colleagues, microgrid operators, and producers of inverter-based control systems will also find useful insights.

3.3 Stakeholder Analysis

The stakeholders relevant for this project are:

- **Problem owner (student and supervisors at RUG):** carry out the research and are responsible for the project outcomes.
- **Academic community:** researchers of power systems and controls who are interested in new insights on inverter-based microgrid models.
- **Microgrid operators and utilities:** responsible for reliable operation of microgrids and directly affected by the functioning of frequency control methods.

- **Inverter and control manufacturers:** companies that design and supply the hardware and algorithms for Droop and VSM Control.
- **Policy makers and regulators:** define technical standards and requirements that shape the conditions under which microgrids operate.
- **End-users and local communities:** benefit greatly from stable electricity but have little influence on technical decisions.

The distribution of these stakeholders by power and interest is shown in Figure 1.

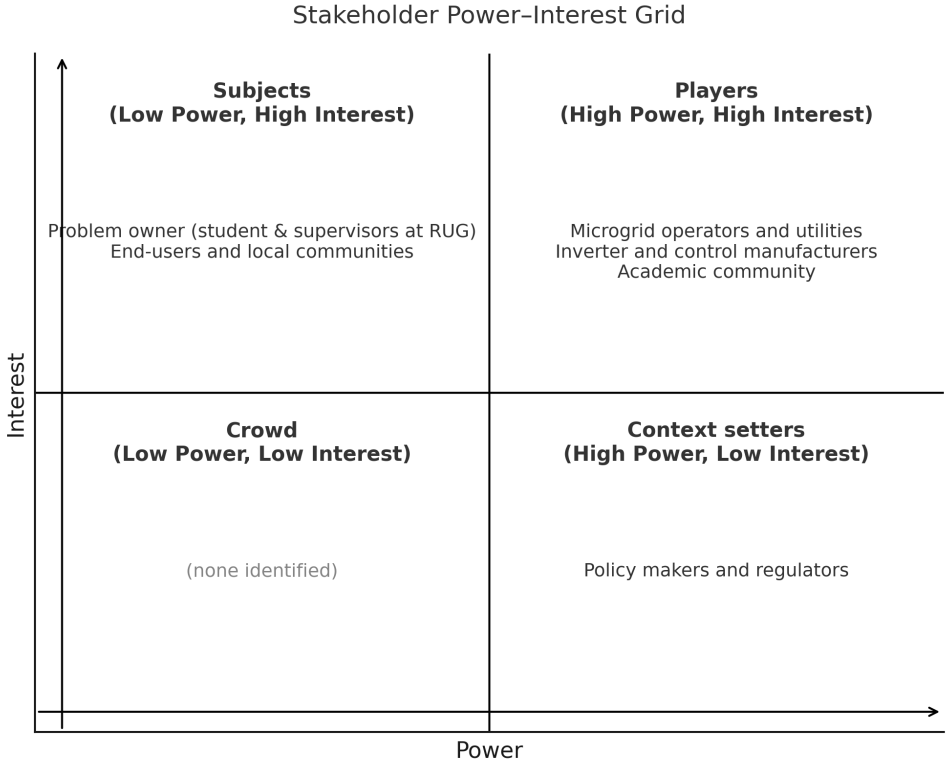

Figure 1: Stakeholder distribution by power and interest.

3.4 Why-What Analysis

A Why-What analysis was created using the ideas discussed in Enserink et al. [6]. This Why-What analysis will serve as a base for the formulation of the research goal and research questions.

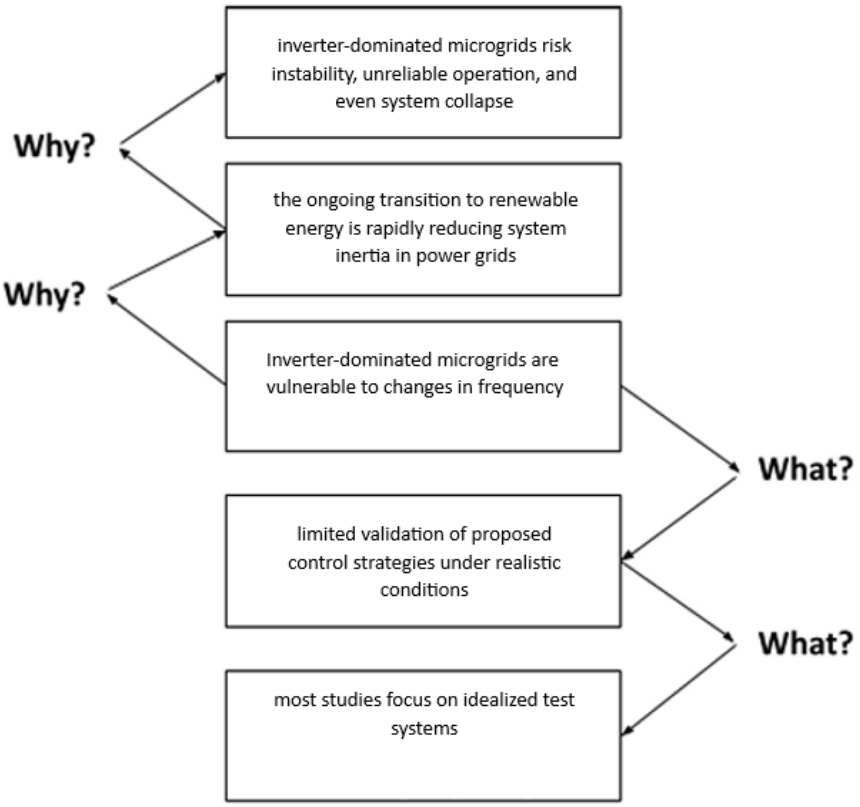

Figure 2: Why-What Analysis of inverter-based microgrids.

4 Research Questions

Following the problem statement and the Why-What analysis, the research questions can be formulated.

Research questions can be distinguished into three types: *research*, *design*, and *validation*. Based on this approach, the following research questions are formulated:

Research Questions

1. What are the fundamental differences in frequency dynamics between traditional synchronous generators, Droop-controlled inverters, VSM-controlled, and Matching-controlled inverters?
2. Which control equations and system representations are needed to develop a MATLAB/Simulink model that captures the frequency dynamics of Droop, VSM, and Matching-controlled inverters in microgrids?

Design Questions

1. How can Droop, VSM, and Matching Control strategies be implemented in MATLAB/Simulink for an islanded inverter-based microgrid?

2. How can disturbances (e.g., load steps, renewable variability, delays) and system parameters be included in the models to reflect realistic operating conditions?

Validation Questions

1. Do the implemented Droop, VSM, and Matching Control strategies produce physically plausible frequency, voltage, and power dynamics in an islanded inverter-based microgrid model when subjected to load step disturbances?

2. How do Droop Control, VSM Control, and Matching Control differ in their dynamic frequency, active power, reactive power, and voltage responses under identical operating conditions and load disturbances?

5 Literature Review

The move from synchronous generators to inverter-based resources changes the system frequency dynamics: synchronous machines have natural inertia while inverters lack this and thus must replicate that behavior via control strategies [1]. Droop Control is the most common and simple approach in inverter-based microgrids, enabling proportional power sharing without communication. [3, 8]

To better match the behavior of synchronous machines, VSM or VSG models implement virtual inertia and damping into inverters [4]. However, these models can be sensitive to parameter choices, operating conditions, and delays in communication channels [9].

In addition to Droop Control and VSM Control, a more recent grid-forming strategy known as Matching Control has been proposed. Matching Control is based on directly matching the internal dynamics of an inverter to those of a synchronous machine, rather than mimicking specific behaviors such as inertia or droop characteristics. The foundational work by Catalin et al. [10] formulates Matching Control by deriving inverter dynamics that reflect the energy and power balance equations of synchronous generators.

Recent studies have expanded traditional frequency control methods with new approaches. Tran et al. propose a distributed virtual inertia control strategy in which multiple distributed energy resources (DERs) operate collectively to provide inertia support while ensuring load sharing [11]. She et al. present virtual inertia scheduling (VIS), which changes inertia and damping settings of inverters in real-time based on economic and operational constraints [12]. Diwan and Linus discuss advanced Droop Control methods which improve power-sharing accuracy, dynamic response, and performance under impedance mismatches [8]. On the modeling side, Al Maruf et al. develop a small-signal model for lossy inverter microgrids that shows the link between voltage and frequency [13]. In addition to this, Gomez Anccas et al. introduce adaptive droop gains, allowing droop coefficients to change dynamically to better handle fluctuations in electricity generation and uncertainty [14].

While the concepts of Droop, VSM and Matching Control are well established, their effectiveness in practical situations has not been fully proven yet. Most studies use simplified models that neglect nonlinearities, delays, or component limits. Hence, this leaves uncertainty about their performance under real disturbances such as load steps or fluctuations in electricity generation. More research is therefore needed to validate and improve the reliability of these control models.

6 Economic Impact and Industrial Relevance

The penetration of renewable energy sources has an economic impact in industrial microgrids. Looking at it from an Industrial Engineering and Management (IEM) perspective, stable frequency control is crucial since it has a direct impact on equipment lifetime, production reliability, and operational costs. Even small frequency changes can shorten the lifetime of motors and other electronics, causing premature failure, leading to unplanned downtime and increased maintenance time needed. Guerrero et al. [15] mentions that poor frequency performance reduces power quality, while Olivares et al. [16] show that power instability will increase operating cost as protection trips and system interruptions are more frequent.

Control Strategies such as VSM and Matching Control support renewable energy penetration as they mimic the behavior of synchronous machines. This enables industries to improve return on investment from photovoltaic panels and battery storage systems. Studies by Arghandeh et al. [17] and Lund et al. [18] show that stability in power grids will reduce fuel consumption and emission-related costs, making stable inverter-based microgrids economically attractive. Further studies by Lasseter [19] show that control strategies like VSM and Matching Control can reduce lifecycle operating costs by 20–30%.

Looking at sectors with critical impact, such as data centers, healthcare, and manufacturing, the economic benefit from stable and reliable power supply is even greater. The result of even small frequency or voltage disturbances can cause data loss, halt production or even have impact on human life in healthcare facilities. Hatziargyriou [20] shows that microgrid economic performance is directly linked to reliability. Hence, having control strategies like VSM and Matching is essential for minimizing disruption.

Mohamed and El-Saadany [21] found that synthetic inertia increases system reliability and minimizes the chance of large-scale blackouts. Hence, improved microgrid control supports national sustainability targets by tackling issues like reduced system inertia, as a result of the increasing penetration of renewable energy sources.

7 Materials and Methods

7.1 Materials

- MATLAB R2025a with Simulink
- Simscape Power Systems toolbox
- Inverter control blocks (Droop and VSM implementations)
- Measurement blocks for frequency, active power, and voltage
- Disturbance modules (step loads)
- Parameter sets for droop coefficients, virtual inertia, and damping constants
- Reference values from peer-reviewed literature

7.2 Methods

This project compares Droop Control, VSM Control, and Matching Control using an inverter-based microgrid model implemented in MATLAB/Simulink. All simulations are performed on the same three-phase system to ensure a consistent and fair comparison.

The microgrid consists of two grid-forming inverters with LCL filters. The complete system model and signal flow are described in Section 9, while the full control strategy implementations are provided in Appendix A.

A load step disturbance is applied to see transient and steady-state behavior. System performance is evaluated using frequency, active and reactive power, RMS voltage, and abc-domain voltage and current responses.

8 Overview of the Control Strategies

Inverter-based microgrids use control strategies that enable distributed energy resources to stabilize voltage and frequency while sharing power. This section provides a simple, yet technical overview of the three control strategies used in this project: Droop Control, VSM Control, and Matching Control. Each method is presented with its governing formulas and parameter definitions.

8.1 Droop Control

Droop Control mimics the steady-state behavior of synchronous generators through relations between power, frequency, and voltage. It does not use dynamic inertia but changes the inverter setpoints based on the measured power.

Power Measurement

The inverter measures output voltage (v_d, v_q) and current (i_d, i_q) in the dq frame and calculates

$$P = \tfrac{3}{2}(v_d i_d + v_q i_q), \qquad Q = \tfrac{3}{2}(v_q i_d - v_d i_q), \tag{1}$$

where P is active power and Q is reactive power.

Frequency Droop

The inverter adjusts its frequency according to:

$$\omega = \omega_0 - m_P(P_f - P_0), \tag{2}$$

with ω_0 = nominal frequency, m_P = active-power droop coefficient, P_0 = nominal active power setpoint.

Voltage Droop

Reactive power affects voltage:

$$V = V_0 - n_Q(Q_f - Q_0), \tag{3}$$

where V_0 = nominal voltage, n_Q = reactive-power droop coefficient, Q_0 = nominal reactive power.

Phase Angle

The phase is obtained through:

$$\theta(k) = \theta(k-1) + T_s\,\omega, \tag{4}$$

where T_s is the sampling period.

Droop Control provides a simple, decentralized power-sharing strategy but has limited transient response in low-inertia microgrids.

8.2 Virtual Synchronous Machine Control

VSM Control introduces synthetic inertia and damping by mimicking the rotational dynamics of a real synchronous generator. This leads to smoother frequency dynamics and better transient response.

Swing Equation

The core dynamic is

$$M\dot{\omega} + D(\omega - \omega_0) = P_m - P_e, \tag{5}$$

where M = virtual inertia, D = virtual damping, ω = inverter frequency, P_m = virtual mechanical power input, P_e = measured electrical output power.

The inverter frequency evolves following:

$$\omega(k) = \omega(k-1) + T_s\,\dot{\omega}. \tag{6}$$

Phase Angle and Internal Voltage

The phase angle is calculated with

$$\theta = \int \omega\, dt. \tag{7}$$

The inverter constructs an internal voltage source:

$$e_{dq} = \begin{bmatrix} E_0 \\ 0 \end{bmatrix}, \tag{8}$$

where E_0 is the internal EMF magnitude.

Voltage and Current Control

The key advantage is that inertia M and damping D shape the frequency response, providing smoother frequency control than Droop Control.

VSM thus stabilizes low-inertia systems by adding virtual energy storage.

8.3 Matching Control

First, the three-phase PCC voltages and currents are transformed to the synchronous dq frame using the internal angle ϕ. The instantaneous active and reactive power at the PCC are computed as

$$P = 1.5\,(v_{od}i_{od} + v_{oq}i_{oq}), \qquad Q = 1.5\,(v_{oq}i_{od} - v_{od}i_{oq}), \tag{9}$$

and passed through a first-order low-pass filter to obtain (P_z, Q_z) with

$$P_z(k) = \alpha P(k) + (1-\alpha)P_z(k-1), \quad Q_z(k) = \alpha Q(k) + (1-\alpha)Q_z(k-1), \quad \alpha = \frac{T_s}{\tau_{PQ} + T_s}. \tag{10}$$

Internal energy-like state update

Matching Control introduces an internal state e_{match} (energy-like variable) with nominal value $E_0 = \frac{1}{2} C_f V_0^2$. Using the filtered electrical power $P_e \triangleq P_z$, the state is updated via

$$\dot{e}_{\text{match}} = (P_0 - P_e) - D_E\,(e_{\text{match}} - E_0), \tag{11}$$

which is discretized in the code as $e_{\text{match}} \leftarrow e_{\text{match}} + T_s \dot{e}_{\text{match}}$. Here, P_0 is the nominal active power setpoint, and D_E provides damping/leakage to prevent drift by pulling e_{match} back toward E_0.

Frequency mapping

The inverter angular frequency reference is obtained from the deviation of e_{match} from E_0,

$$\omega_{\text{ref,raw}} = \omega_0 + K_E\,(e_{\text{match}} - E_0), \tag{12}$$

where K_E determines how strongly the internal energy deviation influences frequency. To avoid high-frequency ripple, the code applies a first-order low-pass filter to $\omega_{\text{ref,raw}}$ with time constant T_w:

$$\omega_{\text{ref}}(k) = \beta_w\,\omega_{\text{ref,raw}}(k) + (1-\beta_w)\,\omega_{\text{ref}}(k-1), \qquad \beta_w = \frac{T_s}{T_w + T_s}, \tag{13}$$

followed by saturation to $[\omega_{\min}, \omega_{\max}]$.

Phase integration

Finally, the internal angle used for all dq transformations and reference generation is updated by integrating the filtered frequency:

$$\phi(k) = \text{mod}(\phi(k-1) + T_s\,\omega_{\text{ref}}(k),\, 2\pi)\,. \tag{14}$$

Voltage / reactive-power handling consistent with the control stack

While Matching Control sets ω_{ref} through the energy-to-frequency mapping above, the voltage reference is maintained in the same form as the other strategies using a Q–V droop relation,

$$v_{sd}^* = V_0 - n_q\,(Q_z - Q_0), \qquad v_{sq}^* = 0, \tag{15}$$

so that reactive power is handled consistently across controllers. The resulting (v_{sd}^*, v_{sq}^*) is then tracked using the same cascaded outer voltage loop, middle grid-side current loop, and inner converter-side current loop. The controller outputs (u_d, u_q) are transformed back to $\alpha\beta$ coordinates using the updated ϕ to form (u_α, u_β) for the PWM modulator.

8.4 Summary

Droop Control is a simple and decentralized control strategy but provides little transient response. VSM adds virtual inertia and damping, improving dynamic frequency response. Matching Control gives inverters synchronous-machine like behavior by making an energy balance, enabling fast and stable transient performance without explicitly modeling inertia and damping.

Together, these methods are the foundation of modern inverter control.

9 Simulink Model

The frequency dynamics of the inverter-based microgrid are analyzed by making use of a MATLAB/Simulink model (see Figure 3). The model includes two identical inverters, which are both connected to a AC bus and supplying a three-phase load to the system. Each inverter is controlled by a controller, modeled as a MATLAB Function block, which recreates the Droop Control strategy mentioned in Section 8.1.

9.1 Overall Topology

On the left side of the model, each inverter is supplied by a 400 V DC source and a IGBT bridge. The inverter is connected to the AC grid through an LCL filter, consisting of:

- converter-side inductance L_f with series resistance R_1,
- shunt filter capacitor C_f,
- grid-side inductance L_g with series resistance R_g.

The outputs of the two filters are linked together to form a three-phase power supply to which a three-phase R–L load is connected.

9.2 Power Stage and Measurements

For each inverter, three sets of three-phase voltages and currents are measured:

- converter-side line currents (i_a, i_b, i_c) flowing through L_f,
- grid-side line currents (i_{oa}, i_{ob}, i_{oc}) at the point of common coupling (PCC),
- capacitor or PCC voltages (v_a, v_b, v_c), and bus voltages (v_{oa}, v_{ob}, v_{oc}).

These measurements are input to the MATLAB function. The MATLAB function calculates the active and reactive power of each inverter and these are connected to scopes for later review.

The entire model has a fixed sampling time of $T_s = 1$ μs, which is also the controller sampling period.

9.3 Grid-Forming Controller Block

The control strategy of the inverters is modeled in the MATLAB FUNCTION block. The function

$$[\alpha\text{-}\beta \text{ voltages}, P_z, Q_z, v_{od}, v_{oq}, i_{od}, i_{oq}] = GFM(v_a, v_b, v_c, i_a, i_b, i_c, i_{oa}, i_{ob}, i_{oc}, v_{oa}, v_{ob}, v_{oc}), \quad (16)$$

outputs the reference voltages u_α, u_β for the PWM modulator, as well as the filtered active and reactive power (P_z, Q_z), the PCC voltages and currents in the dq frame.

Internally, the controller implements three control loops:

1. an outer voltage loop regulating the PCC voltage and generating current references,
2. a middle loop regulating grid-side currents and generating converter-side current references,
3. an inner loop regulating converter-side currents and generating inverter output voltages.

Each loop uses PI controllers with gains derived from desired values for voltage, grid-side current and converter-side current.

9.4 Implementation of Droop Control

The function first defines the parameters of the filter and the controller gains:

$$L_f = 6.3 \text{ mH}, \qquad R_1 = 0.08\ \Omega, \quad (17)$$

$$L_g = 2.2 \text{ mH}, \qquad R_g = 0.05\ \Omega, \quad (18)$$

$$C_f = 4\ \mu\text{F}, \quad (19)$$

and the PI gains of the three loops (`Kpv`, `Kiv`, `Kpio`, `Kiio`, `KpiL`, `KiiL`).

Reference frame transformation. Using the stored phase angle φ, the measured three-phase voltages and currents are transformed from the abc frame to the dq frame:

$$[v_{cd}, v_{cq}] = \text{abc2dq}(v_a, v_b, v_c, \varphi), \qquad [i_d, i_q] = \text{abc2dq}(i_a, i_b, i_c, \varphi), \quad (20)$$

and similarly for the grid currents (i_{od}, i_{oq}) and PCC voltages (v_{od}, v_{oq}). The subfunction `abc2dq` implements the standard Park transformation.

Power calculation and filtering. The active and reactive power at the PCC are computed as

$$P = 1.5\,(v_{od} i_{od} + v_{oq} i_{oq}), \qquad Q = 1.5\,(v_{oq} i_{od} - v_{od} i_{oq}), \quad (21)$$

and low-pass filtered using a first-order discrete filter with time constant τ_{PQ}:

$$P_z(k) = \alpha P(k) + (1-\alpha) P_z(k-1), \qquad Q_z(k) = \alpha Q(k) + (1-\alpha) Q_z(k-1), \quad (22)$$

where $\alpha = T_s/(\tau_{PQ} + T_s)$.

Droop and phase update. The measured powers are put into the droop relations for frequency and voltage:

$$\omega_{\text{ref}} = \omega_0 - m_p (P_z - P_0), \quad (23)$$

$$v_{sd}^* = V_0 - n_q (Q_z - Q_0), \qquad v_{sq}^* = 0, \quad (24)$$

with nominal values $(\omega_0, V_0, P_0, Q_0)$ and droop coefficients m_p, n_q. The internal phase angle is updated as

$$\varphi(k) = \text{mod}\big(\varphi(k-1) + T_s \omega_{\text{ref}},\, 2\pi\big). \quad (25)$$

Cascaded voltage and current loops. The outer voltage loop computes references for the grid currents (i_{od}^*, i_{oq}^*) from the error between reference and measured PCC voltages:

$$e_{vd} = v_{sd}^* - v_{od}, \qquad i_{od}^* = K_{pv} e_{vd} + K_{iv} \int e_{vd}, \tag{26}$$

$$e_{vq} = v_{sq}^* - v_{oq}, \qquad i_{oq}^* = K_{pv} e_{vq} + K_{iv} \int e_{vq}. \tag{27}$$

A feedforward term $j\omega C_f v_c$ is added to take capacitor currents into account. The middle loop generates converter-side current references $(i_{L,d}^*, i_{L,q}^*)$, and the inner loop generates the required inverter output voltages (u_d, u_q).

Output to PWM. Finally, the dq voltages (u_d, u_q) are transformed back to $\alpha\beta$ coordinates,

$$u_\alpha = u_d \cos\varphi - u_q \sin\varphi, \qquad u_\beta = u_d \sin\varphi + u_q \cos\varphi, \tag{28}$$

and supplied to the PWM block which generates the signals for the IGBT bridge.

9.5 Simulation Setup

Both inverters use the same electrical parameters and sampling time. By changing only the control function block (replacing the Droop implementation by a VSM or Matching Control code), the same Simulink model can be reused to compare different control strategies under identical conditions. A three-phase R–L load is connected at the point of common coupling (PCC) and simulates the demand of the islanded microgrid. A load disturbance is applied by a step change in the load parameters at $t = 0.1\,\mathrm{s}$, resulting in increased active and reactive power demand. The disturbance is applied to all three phases, ensuring that the system response is only caused by the control strategy.

10 Comparison of Control Strategies

This section compares the performance of Droop Control, VSM Control, and Matching Control based on their dynamic response in terms of active and reactive power, as well as voltage and current waveforms. All detailed time-domain plots are provided in Appendix B. The discussion in this section refers to these figures to highlight the main observed trends.

The comparison focuses on the system response to a step change in load, applied at $t = 0.1\,\mathrm{s}$.

10.1 Droop Control Results

10.1.1 Frequency Response

Figure 8 shows the system frequency response under Droop Control. Prior to the load disturbance, the frequency remains close to the nominal value of 50 Hz, with only small oscillations during the initial synchronization process.

Following the load step at $t \approx 0.1\,\mathrm{s}$, the frequency exhibits a clearly oscillatory transient. A first positive deviation is observed, with the frequency peaking at approximately 50.07–50.08 Hz, after which a sequence of alternating overshoots and undershoots occurs. The most pronounced frequency dip reaches approximately 49.90 Hz, indicating a relatively deep temporary frequency drop.

These oscillations decay gradually, and the frequency converges to a new steady state value slightly below nominal, around 49.97–49.98 Hz. This steady state error is a direct result of the nature of Droop Control, as the controller intentionally trades frequency accuracy for proportional load sharing. Overall, the Droop-controlled system demonstrates a fast but lightly damped frequency response.

10.1.2 Active Power Response

The active power response of the inverter is shown in Figure 4. During the initial start-up phase ($t < 0.05\,\mathrm{s}$), the output power smoothly increases from zero toward the nominal operating point of approximately 1800 W, without excessive overshoot.

At the load change occurring at $t \approx 0.1\,\mathrm{s}$, a small but clearly visible dip in active power is observed, with the instantaneous value dropping to roughly 1799.98 W. This dip coincides with the frequency excursion discussed earlier and reflects the link between active power and frequency inherent to Droop Control.

After this transient, the active power recovers quickly and reaches a slightly higher steady state value, consistent with the increased load demand. The settling behavior is smooth, with minimal oscillations in steady state, indicating stable active power sharing.

10.1.3 Reactive Power Response

Figure 5 presents the reactive power response under Droop Control. During start-up, the reactive power rises toward its nominal value of approximately 300 var, accompanied by a small oscillatory transient.

At the moment of the load increase ($t \approx 0.1\,\mathrm{s}$), a small reactive power dip is observed, followed by a modest overshoot. The magnitude of this deviation remains limited, within a narrow band of only a few tenths of a var around the nominal operating point.

After the transient, the reactive power converges smoothly to a new steady state value slightly above 300 var. This confirms that the implemented Q–V droop successfully regulates reactive power while maintaining voltage stability.

10.1.4 RMS Voltage Response

The RMS voltage at the point of common coupling is shown in Figure 9. During the initial transient, the voltage rises monotonically toward its nominal level of approximately $110\,\mathrm{V_{RMS}}$. No significant overshoot is observed during this phase.

Following the load step at $t \approx 0.1\,\mathrm{s}$, a small voltage dip occurs, reflecting the increased reactive power demand. The voltage deviation remains limited and recovers quickly, settling at a slightly reduced steady state value consistent with the Q–V droop characteristic.

10.1.5 Voltage and Current Waveforms

Figures 6 and 7 show the three-phase voltage and current waveforms in the time domain. After an initial synchronization transient, the waveforms become well balanced and sinusoidal, indicating correct phase alignment and stable operation.

The current magnitude increases noticeably after the load step, while the voltage waveform remains largely unchanged in shape. No significant waveform distortion or instability is observed

following the transient.

10.2 VSM Control Results

10.2.1 Frequency Response

The frequency response under VSM Control is shown in Figure 14. Prior to the load change, the frequency remains regulated around the nominal value of 50 Hz. Following the disturbance at $t = 0.1\,\text{s}$, the frequency exhibits an oscillatory transient with a first positive peak of approximately 50.08–50.10 Hz, followed by a negative excursion down to about 49.95 Hz. The oscillations are gradually damped, and the frequency converges to a steady state value slightly below nominal, around 49.97–49.98 Hz.

Compared to the Droop Control, the VSM frequency response shows a similar oscillatory structure but with slightly smoother damping, which can be the result of the virtual inertia and damping terms introduced by the swing-equation.

10.2.2 Active Power response

The active power response is shown in Figure 10. During the initial start-up , the active power increases smoothly toward its nominal operating point of approximately 1800 W. At $t = 0.1\,\text{s}$, the load increase causes a short power dip of roughly 10–15 W, after which the active power recovers smoothly.

The settling after the load increase is well damped, with the power reaching its new steady state value within approximately 40–50 ms. No oscillations are observed in steady state, indicating stable power sharing behavior under VSM Control.

10.2.3 Reactive Power Response

Figure 11 shows the reactive power behavior. The reactive power rises gradually during start-up and stabilizes close to its reference value of approximately 300 var. When the load change occurs at $t = 0.1\,\text{s}$, a small transient deviation is observed, followed by a smooth recovery with no oscillations.

The reactive power response shows limited overshoot and low oscillatory behavior, showing the effectiveness of the Q–V control mechanism when combined with the VSM dynamics.

10.2.4 RMS Voltage Response

The RMS voltage response at the point of common coupling is shown in Figure 15. Starting from zero, the voltage increases smoothly during the start-up phase and reaches its nominal level of approximately $110\,\text{V}_{\text{RMS}}$. At the instant of the load disturbance, a small voltage dip can be seen, but the voltage recovers rapidly and settles close to its nominal value.

10.2.5 Voltage and Current Waveforms

Figures 12 and 13 show the three-phase voltage and current waveforms in the time domain. After an initial synchronization transient, the waveforms become well balanced and sinusoidal, indicating correct phase alignment and stable operation.

The current magnitude increases noticeably after the load step, while the voltage waveform remains largely unchanged in shape. No significant waveform distortion or instability is observed following the transient.

10.3 Matching Control Results

10.3.1 Frequency Response

Figure 20 presents the frequency response of the microgrid under Matching Control. Prior to the load disturbance, the frequency remains regulated around the nominal value of 50 Hz. Following the load increase at $t = 0.1\,\mathrm{s}$, the frequency response differs fundamentally from that observed under Droop and VSM Control.

Rather than having a positive overshoot, the frequency shows a dominant negative dip, reaching a minimum of approximately 49.90 Hz. This initial dip is followed by a smooth recovery with only minor oscillatory behavior. The frequency then converges monotonically toward a new steady state value close to 49.95 Hz. Compared to Droop-based approaches, the response is less oscillatory and more heavily damped, however the minimum frequency deviation is slightly larger.

This behavior reflects the energy-based mechanism of Matching Control, where frequency dynamics are governed by the balance between supplied and demanded power rather than by an explicit droop slope or swing equation.

10.3.2 Active Power Response

The active power response under Matching Control is shown in Figure 16. During start-up, the inverter output power increases smoothly toward the nominal operating point. At the load change instant, a brief transient is observed, after which the active power rises steadily to meet the increased demand.

The transition is notably smooth, with minimal overshoot and limited oscillatory behavior. Compared to Droop and VSM Control, the active power trajectory under Matching Control shows a more monotonic convergence, indicating improved damping.

10.3.3 Reactive Power Response

Figure 17 illustrates the reactive power behavior. The reactive power increases smoothly during start-up and remains close to its nominal value prior to the disturbance. After the load increase, a small transient deviation occurs, followed by a smooth transition to a slightly higher steady state value.

Oscillations in reactive power are noticeably smaller than those observed under Droop and VSM Control, highlighting the stabilizing effect of the energy-based control mechanism.

10.3.4 RMS Voltage Response

The RMS voltage response is shown in Figure 21. The voltage rises smoothly during start-up and remains well regulated throughout the simulation. A minor voltage dip is visible following the load increase, after which the voltage quickly recovers and settles near its nominal value.

10.3.5 Voltage and Current Waveforms

The three-phase voltage and current waveforms, presented in Figures 18 and 19, remain balanced and sinusoidal. Only minor transient distortions are observed around the disturbance, confirming stable grid-forming operation under Matching Control.

11 Discussion

The simulation results provide clear insights into the differences between Droop Control, VSM Control, and Matching Control. Although all three strategies have stable operation after a load disturbance, their transient behavior and frequency regulation differ.

11.1 Frequency Dynamics

The frequency response of Droop Control has fast but oscillatory transient behavior following the load increase. As can be seen in the frequency plots, the Droop-controlled system shows an initial positive overshoot above the nominal frequency, followed by a large undershoot and several damped oscillations before reaching a new steady state slightly below the nominal frequency of 50 Hz. This behavior is a good example of Droop-based Control, as frequency deviations are directly linked and proportional to active power changes. Even though Droop Control provides an effective primary frequency response, it introduces frequency error and limited damping after load disturbances.

The VSM Control strategy has a frequency response that is similar to that of Droop Control. The addition of virtual inertia and damping, however, result in smoother transient behavior, but the overall response still has oscillatory behavior with similar overshoot and settling time. The measured frequency dip and steady state error are very similar to those under Droop Control.

In contrast to the above strategies, Matching Control has a different frequency response. Rather than oscillating around the nominal value, the frequency response is dominated by a single, deeper dip followed by a smooth and well-damped recovery. No overshoot above 50 Hz can be seen. This behavior reflects the energy-based part of Matching Control, where frequency response is linked to the stored energy instead of a droop slope or swing equation. Even though the minimum frequency deviation is slightly larger than in the Droop and VSM simulations, the reduced oscillatory behavior shows improved damping and potentially lower impact on grid-connected equipment.

11.2 Active and Reactive Power Response

The active power responses show the differences between the control strategies even more. Under Droop Control, the active power shows a fast and sharp transient dip after which the active power is increased to a new steady state. The reactive power has a fast and sharp dip, followed by some oscillatory behavior before reaching a new steady state. Both of the steady states are higher than before the load increase.

Under VSM Control, the increase in active and reactive power differs substantially from the Droop Controlled system. Whereas Droop Control showed a fast and sharp dip after the load increase, VSM has a much smoother behavior with almost no decrease. The active power and reactive power reach their new steady state much smoother with no oscillations shown.

Matching Control produces a similar active power trajectory. After the load increase, the active power smoothly reaches its new steady state value with no oscillations. The reactive power

response of Matching Control is also similar to that of VSM, a new steady state is reached smoothly with no oscillations.

11.3 Voltage and Current Behavior

The RMS voltage profiles show that all three control strategies keep reliable voltage regulation after the disturbance. Small voltage dips are seen at the instant of the load increase, but these are quickly corrected. Matching Control has a slightly smoother voltage recovery.

The voltage and current waveforms in the abc reference frame are stable in all cases. After a brief synchronization transient, which can be seen in the beginning of the plots, the three-phase voltages remain balanced and sinusoidal. The current magnitude increases following the load step as expected, with no signs of instability. This indicates that current and voltage regulation are sufficiently robust for all three strategies.

11.4 Implications for Inverter-Dominated Microgrids

The results show the difference between simplicity and dynamic performance in a system context. Droop Control remains a common solution due to its simplicity and proven reliability, but its oscillatory response and steady state deviation may limit performance in low-inertia microgrids. VSM Control provides a more natural framework by simulating synchronous generator dynamics. Nonetheless, its advantages over Droop Control are heavily dependent on parameter tweaking.

Matching Control appears as a good alternative as it completely changes the synchronization methods. The smoother frequency and power responses indicate improved damping and less oscillatory behavior, which could be useful in future inverter-based systems. However, the deeper frequency dip found in the simulations shows the significance of careful parameter selection to balance damping, responsiveness, and frequency stability.

The analysis confirms that even though all three strategies will have stable grid-forming operation, their dynamic behavior differs. The choice of control strategy should therefore be guided by the specific requirements of the microgrid, including allowable frequency deviation, transient performance, and implementation complexity.

12 Conclusion

This project used Droop Control, VSM Control, and Matching Control to compare the frequency dynamics of inverter-based microgrids. In order to assess the three control strategies under the same electrical parameters and disturbance conditions, a MATLAB/Simulink model of an islanded microgrid was built. With special attention to frequency behavior, power dynamics, voltage regulation, and waveform quality, the analysis concentrated on how the system responded to a step increase in load.

The findings show that while classical Droop Control offers a quick primary frequency response, it has a persistent steady state frequency offset and lightly damped oscillatory transients. Compared to Droop Control, VSM Control produces somewhat smoother frequency dynamics while maintaining a similar overall response structure by introducing virtual inertia and damping. However, active and reactive power responses are much smoother with VSM Control. When inertia and damping are not aggressively tuned, the VSM behavior stays mostly droop-like under the selected parameter settings, supporting theoretical documents in the literature.

The synchronization mechanism used by Matching Control is completely different. Frequency

is controlled by an energy-based balance between supplied and demanded power rather than explicit droop or swing-equation dynamics. As a result, there is much less oscillatory behavior in the frequency response, which is dominated by a single drop followed by a smooth, well-damped recovery. Improved damping and stability are indicated by more monotonic active and reactive power responses under Matching Control. All three strategies maintain strong voltage regulation and waveform quality, indicating correct grid-forming operation.

Overall, the study shows that Matching Control provides better transient response and damping. While Droop and VSM Control are still practical and simple solutions, Matching Control is a viable option for low-inertia microgrids with high renewable energy penetration because of better transient response. Further work could expand this analysis taking into account communication delays, multiple inverters with different ratings, and parameter sensitivity.

References

[1] B. Hartmann, I. Vokony, and I. Taczi, "Effects of decreasing synchronous inertia on power system dynamics—overview of recent experiences and marketisation of services," *International Transactions on Electrical Energy Systems*, vol. 29, 07 2019.

[2] B. A. Bastiani and R. V. de Oliveira, "Frequency dynamics of power systems with inertial response support from wind generation," *Energies*, vol. 16, no. 14, p. 5280, 2023.

[3] S. D'Arco and J. A. Suul, "Equivalence of virtual synchronous machines and frequency-droops for converter-based microgrids," *IEEE Transactions on Smart Grid*, vol. 5, no. 1, pp. 394–395, 2014.

[4] V. Mallemaci, F. Mandrile, S. Rubino, A. Mazza, E. Carpaneto, and R. Bojoi, "A comprehensive comparison of virtual synchronous generators with focus on virtual inertia and frequency regulation," *Electric Power Systems Research*, vol. 201, p. 107516, 12 2021.

[5] A. Ademola-Idowu and B. Zhang, "Optimal design of virtual inertia and damping coefficients for virtual synchronous machines," 06 2018.

[6] B. Enserink, P. Bots, E. Daalen, L. Hermans, J. Koppenjan, R. Kortmann, J. Kwakkel, J. Slinger, T. Ploeg, and W. Thissen, *Policy Analysis of Multi-Actor Systems*, 08 2022.

[7] F. Ackermann and C. Eden, "Strategic management of stakeholders: Theory and practice," *Long Range Planning*, vol. 44, pp. 179–196, 06 2011.

[8] S. Diwan and R. Linus, "Advanced droop control strategies for microgrid," *International Journal of Electrical and Electronics Engineering*, vol. 11, pp. 335–360, 12 2024.

[9] C. Zhou, Y. Liao, K. Zhang, X. Xu, and J. Liao, "Virtual inertia based hierarchical control scheme for distributed generations considering communication delay," *Frontiers in Energy Research*, vol. Volume 11 - 2023, 2023.

[10] C. Arghir, T. Jouini, and F. Dörfler, "Grid-forming control for power converters based on matching of synchronous machines," *Automatica*, vol. 95, pp. 273–282, 2018.

[11] T. Tran, A. Nguyen, M.-Q. Tran, D. Ngo, and P. Nguyen, "Distributed virtual inertia control for frequency regulation in islanded microgrids," 11 2023, pp. 1–5.

[12] B. She, F. Li, H. Cui, J. Wang, Q. Zhang, and R. Bo, "Virtual inertia scheduling (vis) for real-time economic dispatch of ibr-penetrated power systems," *IEEE Transactions on Sustainable Energy*, vol. 15, no. 2, pp. 938–951, 2024.

[13] A. A. Maruf, A. Dubey, and S. Roy, "Small-signal dynamics of lossy inverter-based microgrids for generalized droop controls," in *2024 IEEE 63rd Conference on Decision and Control (CDC)*, 2024, pp. 5359–5366.

[14] E. Gomez Anccas, C. Hans, and D. Schulz, "Microgrid operation control with adaptable droop gains," 10 2025, pp. 1–5.

[15] J. C. Vasquez, J. Guerrero, J. Miret, M. Castilla, and L. Vicuna, "Hierarchical control of intelligent microgrids," *Industrial Electronics Magazine, IEEE*, vol. 4, pp. 23 – 29, 01 2011.

[16] D. E. Olivares, A. Mehrizi-Sani, A. H. Etemadi, C. A. Cañizares, R. Iravani, M. Kazerani, A. H. Hajimiragha, O. Gomis-Bellmunt, M. Saeedifard, R. Palma-Behnke, G. A. Jiménez-Estévez, and N. D. Hatziargyriou, "Trends in microgrid control," *IEEE Transactions on Smart Grid*, vol. 5, no. 4, pp. 1905–1919, 2014.

[17] R. Arghandeh, A. von Meier, L. Mehrmanesh, and L. Mili, "On the definition, modeling, and control of microgrids," *Renewable and Sustainable Energy Reviews*, vol. 41, pp. 123–134, 2015.

[18] P. D. Lund, J. Lindgren, J. Mikkola, and J. Salpakari, "Review of energy system flexibility measures to enable high levels of variable renewable electricity," *Renewable and Sustainable Energy Reviews*, vol. 45, pp. 785–807, 2015.

[19] R. H. Lasseter, "Smart distribution: Coupled microgrids," *Proceedings of the IEEE*, vol. 99, no. 6, pp. 1074–1082, 2011.

[20] N. D. Hatziargyriou, *Microgrids: Architectures and Control*, 01 2014.

[21] Y. Mohamed and E. El-Saadany, "Adaptive decentralized droop controller to preserve power sharing stability of paralleled inverters in distributed generation microgrids," *IEEE Transactions on Power Electronics*, vol. 23, no. 6, pp. 2806–2816, 2008.

Gen-AI usage: ChatGPT model GPT-5.2 was used in this report for brainstorming, language correction, and assistance with coding in MATLAB.

A Simulink Model and MATLAB Implementation

This appendix presents the detailed implementation of the Simulink model used in this project, including the grid-forming inverter structure and the MATLAB code used to implement the control strategies.

A.1 Simulink Model Overview

Figure 3 shows the complete Simulink model of the inverter-based microgrid. The model consists of two grid-forming inverters connected through LCL filters to a common AC bus supplying a three-phase load.

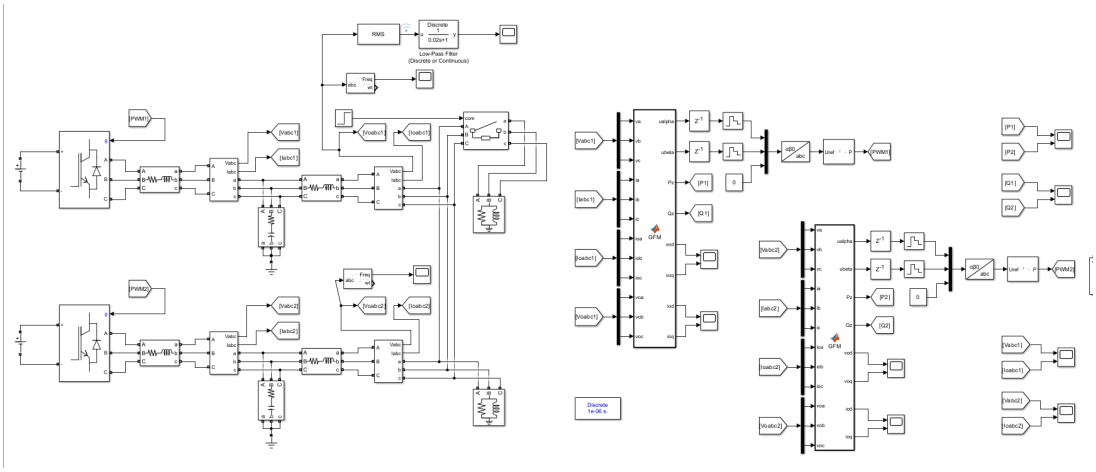

Figure 3: Overview of the Simulink microgrid model.

A.2 Droop Control Implementation

The Droop-based grid-forming controller is implemented using a MATLAB Function block. The full source code is provided below for completeness.

```
function [ualpha, ubeta, Pz, Qz, vod, voq, iod, ioq] = ...
    GFM(va, vb, vc, ia, ib, ic, ioa, iob, ioc, voa, vob, voc)

%% ---------- Params ----------
w0 = 2*pi*50;
Lf = 6.3e-3;     R1 = 0.08;       % inverter side Lf,R
Lg = 2.2e-3;     Rg = 0.05;       % grid side Lg,R
Cf = 4e-6;

% Out loop: from uo to io, f_v      20~40 Hz
Kpv = 0.01;      Kiv = 6;

% Middle loop: from io to iL, f_io      150~300 Hz
Kpio = 2*pi*200*Lg;      %      2.77
Kiio = 2*pi*200*Rg;      %      62.8

% Inner loop: from iL to uo, f_iL      800~1500 Hz
KpiL = 2*pi*1200*Lf;     %      47.5
KiiL = 2*pi*1200*R1;     %      603

% Droop
V0 = 110*sqrt(2);
```

```
P0 = 1800;
Q0 = 300;
mp = 2*pi*0.2/600;
nq = 2/150;

tauPQ  = 0.02;
Ts = 1e-6;
alpha  = Ts/(tauPQ+Ts);

%% ---------- States ----------
persistent ivd ivq iiod iioq iild iilq ph Pz1 Qz1
if isempty(ivd),  ivd=0; ivq=0; end
if isempty(iiod), iiod=0; iioq=0; end
if isempty(iild), iild=0; iilq=0; end
if isempty(ph),   ph=0;  end
if isempty(Pz1),  Pz1=P0; Qz1=Q0; end

%% ---------- dq transforms ----------
[vcd, vcq] = abc2dq(va, vb, vc, ph);     % vC
[id,  iq ] = abc2dq(ia, ib, ic, ph);     % iL
[iod, ioq] = abc2dq(ioa,iob,ioc,ph);     % io
[vod, voq] = abc2dq(voa,vob,voc,ph);     % PCC

%% ---------- P/Q at PCC (LPF) ----------
P = 1.5*(vod*iod + voq*ioq);
Q = 1.5*(voq*iod - vod*ioq);
Pz = alpha*P + (1-alpha)*Pz1;
Qz = alpha*Q + (1-alpha)*Qz1;

%% ---------- Droop & phase ----------
wref = w0 - mp*(Pz - P0);
vsd_ref = V0 - nq*(Qz - Q0);
vsq_ref = 0;
ph = mod(ph + Ts*wref, 2*pi);

%% ---------- dq 2      ----------
ualpha = ud*cos(ph) - uq*sin(ph);
ubeta = ud*sin(ph) + uq*cos(ph);

%% ---------- utils: abc2dq ----------
function [d,q] = abc2dq(a,b,c,th)
    c0 = cos(th);   s0 = sin(th);
    c1 = cos(th-2*pi/3);    s1 = sin(th-2*pi/3);
    c2 = cos(th+2*pi/3);    s2 = sin(th+2*pi/3);
    d = (2/3)*(c0*a + c1*b + c2*c);
    q = (2/3)*(-s0*a - s1*b - s2*c);
end
end
```

Listing 1: Droop-based Grid-Forming Controller

A.3 VSM and Matching Control Implementations

Similarly, the VSM and Matching Control strategies are implemented by modifying the frequency and angle-generation logic within the same controller structure. The corresponding MATLAB functions are listed below.

```
function [ualpha, ubeta, Pz, Qz, vod, voq, iod, ioq] = ...
    GFM(va, vb, vc, ia, ib, ic, ioa, iob, ioc, voa, vob, voc)

%% ---------- Parameters ----------
```

```
w0 = 2*pi*50;
P0 = 1800;    % nominal active power (W)
Lf = 6.3e-3;  R1 = 0.08;
Lg = 2.2e-3;  Rg = 0.05;
Cf = 4e-6;

% Voltage loop
Kpv = 0.01;
Kiv = 6;

% Current loops
Kpio = 2*pi*200*Lg;
Kiio = 2*pi*200*Rg;
KpiL = 2*pi*1200*Lf;
KiiL = 2*pi*1200*R1;

% Nominal voltage
V0 = 110*sqrt(2);

%  Q V  droop
nq = 2/150;

% Power filter
tauPQ = 0.02;
Ts    = 1e-6;
alpha  = Ts/(tauPQ+Ts);

% ---------- VSM parameters ----------
Mvirt = 0.8;     % virtual inertia
Dvirt = 800;     % virtual damping

% Frequency limits
wmax = 2*pi*50.5;
wmin = 2*pi*49.5;

%% ---------- States ----------
persistent ivd ivq iiod iioq iild iilq ph Pz1 Qz1 w_virt startup_done
if isempty(ivd), ivd=0; ivq=0; end
if isempty(iiod), iiod=0; iioq=0; end
if isempty(iild), iild=0; iilq=0; end
if isempty(ph), ph=0; end
if isempty(Pz1), Pz1=0; Qz1=0; end
if isempty(w_virt), w_virt=w0; end
if isempty(startup_done), startup_done=false; end

%% ---------- Initial phase alignment ----------
if ~startup_done
    [v_alpha, v_beta] = abc2alphabeta(voa, vob, voc);
    ph = atan2(v_beta, v_alpha);
    w_virt = w0;
    startup_done = true;
end

%% ---------- dq transforms ----------
[vcd, vcq] = abc2dq(va, vb, vc, ph);
[id,  iq ] = abc2dq(ia, ib, ic, ph);
[iod, ioq] = abc2dq(ioa,iob,ioc,ph);
[vod, voq] = abc2dq(voa,vob,voc,ph);

%% ---------- Instantaneous P/Q ----------
P = 1.5*(vod*iod + voq*ioq);
Q = 1.5*(voq*iod - vod*ioq);

```

```
%% ---------- Filtered P/Q ----------
Pz = alpha*P + (1-alpha)*Pz1;
Qz = alpha*Q + (1-alpha)*Qz1;
Pz1 = Pz;
Qz1 = Qz;

%% ---------- VSM CONTROL ----------
Pe = Pz;

% Swing equation
domega = (P0 - Pe - Dvirt*(w_virt - w0)) / Mvirt;
w_virt = w_virt + Ts*domega;
wref   = w_virt;

% Frequency limits
if wref > wmax
    wref = wmax;
elseif wref < wmin
    wref = wmin;
end

%% ---------- Voltage reference ----------
vsd_ref = V0 - nq*(Qz);
vsq_ref = 0;

% Phase update
ph = mod(ph + Ts*wref, 2*pi);

%% ---------- Voltage loop ----------
evd = vsd_ref - vod;
evq = vsq_ref - voq;
ivd = ivd + Ts*evd;
ivq = ivq + Ts*evq;
iod_ref = Kpv*evd + Kiv*ivd;
ioq_ref = Kpv*evq + Kiv*ivq;

%% ---------- Output current loop ----------
icd_ff = - wref * Cf * vcq;
icq_ff = + wref * Cf * vcd;

eiod = iod_ref - iod;
eioq = ioq_ref - ioq;
iiod = iiod + Ts*eiod;
iioq = iioq + Ts*eioq;

iLref_d = iod_ref + icd_ff + (Kpio*eiod + Kiio*iiod);
iLref_q = ioq_ref + icq_ff + (Kpio*eioq + Kiio*iioq);

%% ---------- Inductor current loop ----------
eild = iLref_d - id;
eilq = iLref_q - iq;
iild = iild + Ts*eild;
iilq = iilq + Ts*eilq;

ud = vcd + R1*id + (KpiL*eild + KiiL*iild) + wref*Lf*iq;
uq = vcq + R1*iq + (KpiL*eilq + KiiL*iilq) - wref*Lf*id;

%% ---------- dq           ----------
ualpha = ud*cos(ph) - uq*sin(ph);
ubeta  = ud*sin(ph) + uq*cos(ph);

%% ---------- Utilities ----------
function [d,q] = abc2dq(a,b,c,th)
```

```
    d = (2/3)*(cos(th)*a + cos(th-2*pi/3)*b + cos(th+2*pi/3)*c);
    q = (2/3)*(-sin(th)*a - sin(th-2*pi/3)*b - sin(th+2*pi/3)*c);
end

function [alpha, beta] = abc2alphabeta(a,b,c)
    alpha = (2/3)*(a - 0.5*b - 0.5*c);
    beta  = (2/3)*(sqrt(3)/2*(b - c));
end

end
```

Listing 2: Virtual Synchronous Machine (VSM) control implemented in MATLAB

```
function [ualpha, ubeta, Pz, Qz, vod, voq, iod, ioq] = ...
    GFM(va, vb, vc, ia, ib, ic, ioa, iob, ioc, voa, vob, voc)

%% ---------- Parameters ----------
w0 = 2*pi*50;

Lf = 6.3e-3;    R1 = 0.08;
Lg = 2.2e-3;    Rg = 0.05;
Cf = 4e-6;

% Voltage and current control loops
Kpv = 0.01;     Kiv = 6;
Kpio = 2*pi*200*Lg;
Kiio = 2*pi*200*Rg;
KpiL = 2*pi*1200*Lf;
KiiL = 2*pi*1200*R1;

% Nominal setpoints
V0 = 110*sqrt(2);
P0 = 1800;
Q0 = 300;

%  Q V  droop
nq = 2/150;

% Power filtering
tauPQ = 0.02;
Ts    = 1e-6;
alpha = Ts/(tauPQ+Ts);

%% ---------- Matching Control Parameters ----------
E0    = 0.5*Cf*V0^2;
K_E   = 40;
D_E   = 800;
T_w   = 0.01;

wmax = 2*pi*50.5;
wmin = 2*pi*49.5;

%% ---------- States ----------
persistent ivd ivq iiod iioq iild iilq ph Pz1 Qz1 e_match wref_f startup_done
if isempty(ivd), ivd=0; ivq=0; end
if isempty(iiod), iiod=0; iioq=0; end
if isempty(iild), iild=0; iilq=0; end
if isempty(ph), ph=0; end
if isempty(Pz1), Pz1=P0; Qz1=Q0; end
if isempty(e_match), e_match=E0; end
if isempty(wref_f), wref_f=w0; end
if isempty(startup_done), startup_done=false; end

%% ---------- dq transforms ----------
```

```
[vcd, vcq] = abc2dq(va, vb, vc, ph);
[id, iq]   = abc2dq(ia, ib, ic, ph);
[iod, ioq] = abc2dq(ioa, iob, ioc, ph);
[vod, voq] = abc2dq(voa, vob, voc, ph);

%% ---------- Active and reactive power ----------
P = 1.5*(vod*iod + voq*ioq);
Q = 1.5*(voq*iod - vod*ioq);

Pz = alpha*P + (1-alpha)*Pz1;
Qz = alpha*Q + (1-alpha)*Qz1;
Pz1 = Pz;
Qz1 = Qz;

%% ---------- Matching Control Law ----------
Pe = Pz;

de = (P0 - Pe) - D_E*(e_match - E0);
e_match = e_match + Ts*de;

wref_raw = w0 + K_E*(e_match - E0);
beta_w = Ts/(T_w + Ts);
wref_f = beta_w*wref_raw + (1-beta_w)*wref_f;
wref = min(max(wref_f, wmin), wmax);

%% ---------- Voltage reference ----------
vsd_ref = V0 - nq*(Qz - Q0);
vsq_ref = 0;
ph = mod(ph + Ts*wref, 2*pi);

%% ---------- Control loops ----------
evd = vsd_ref - vod;
evq = vsq_ref - voq;
ivd = ivd + Ts*evd;
ivq = ivq + Ts*evq;
iod_ref = Kpv*evd + Kiv*ivd;
ioq_ref = Kpv*evq + Kiv*ivq;

icd_ff = - wref * Cf * vcq;
icq_ff = + wref * Cf * vcd;

eiod = iod_ref - iod;
eioq = ioq_ref - ioq;
iiod = iiod + Ts*eiod;
iioq = iioq + Ts*eioq;

iLref_d = iod_ref + icd_ff + (Kpio*eiod + Kiio*iiod);
iLref_q = ioq_ref + icq_ff + (Kpio*eioq + Kiio*iioq);

eild = iLref_d - id;
eilq = iLref_q - iq;
iild = iild + Ts*eild;
iilq = iilq + Ts*eilq;

ud = vcd + R1*id + (KpiL*eild + KiiL*iild) + wref*Lf*iq;
uq = vcq + R1*iq + (KpiL*eilq + KiiL*iilq) - wref*Lf*id;

%% ---------- dq to alpha-beta ----------
ualpha = ud*cos(ph) - uq*sin(ph);
ubeta  = ud*sin(ph) + uq*cos(ph);

%% ---------- Utility functions ----------
function [d,q] = abc2dq(a,b,c,th)
```

```
    d = (2/3)*(cos(th)*a + cos(th-2*pi/3)*b + cos(th+2*pi/3)*c);
    q = (2/3)*(-sin(th)*a - sin(th-2*pi/3)*b - sin(th+2*pi/3)*c);
end

end
```

Listing 3: Matching Control implementation with nominal power setpoint P_0

B Simulation Waveforms

This appendix contains the time-domain simulation results used to evaluate the different grid-forming control strategies. All figures correspond to the same load disturbance.

B.1 Droop Control Results

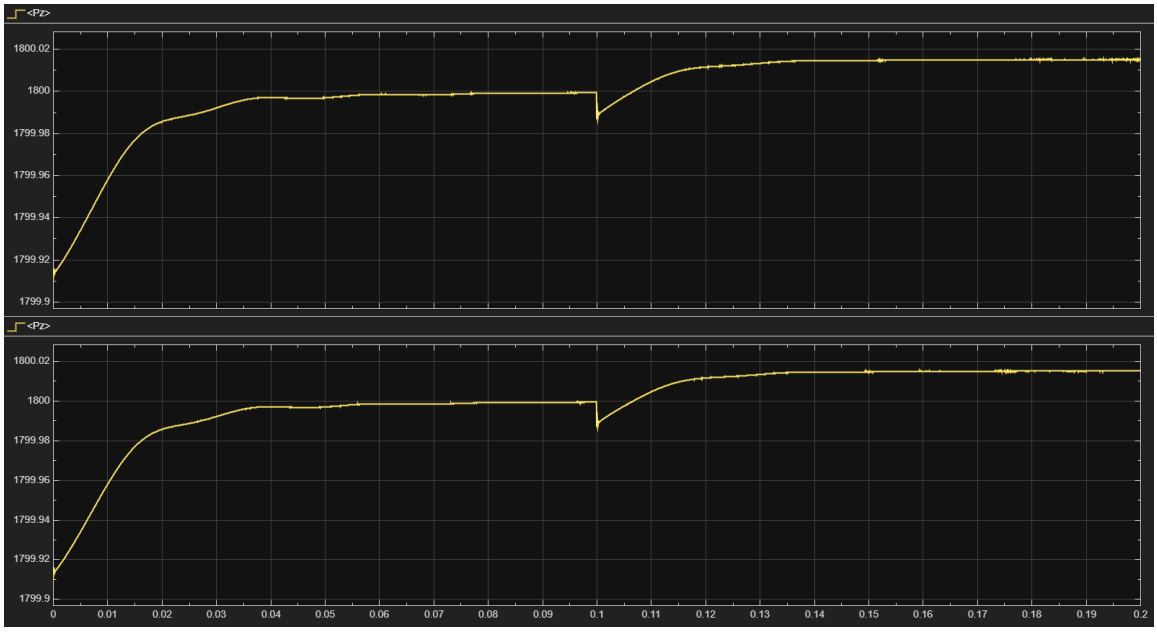

Figure 4: Active power response under Droop Control.

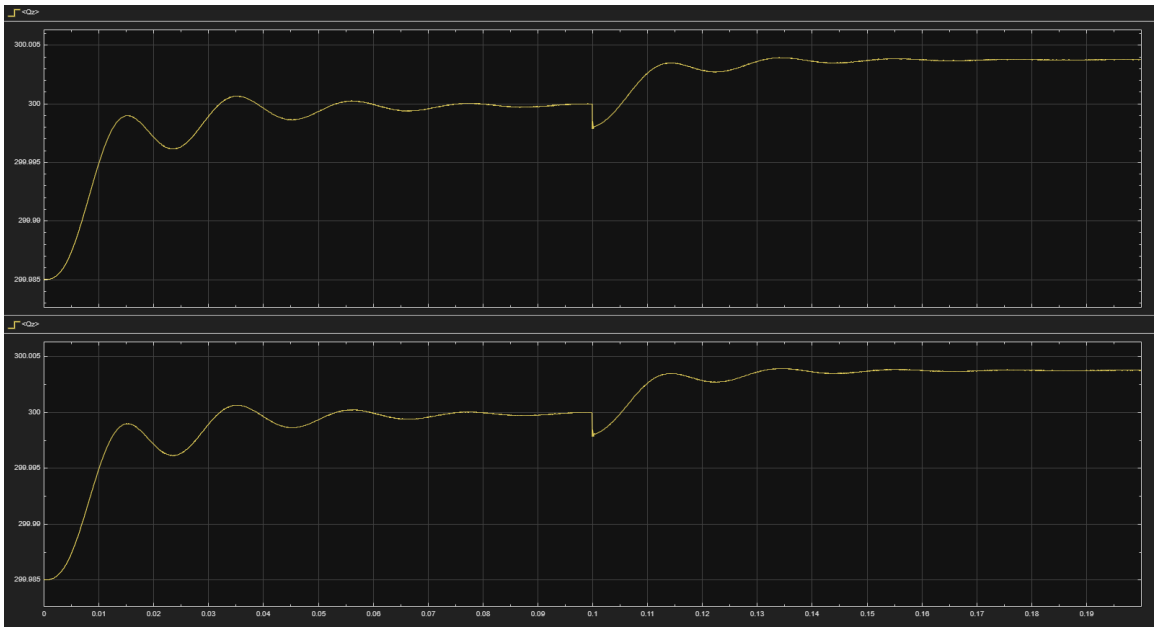

Figure 5: Reactive power response under Droop Control.

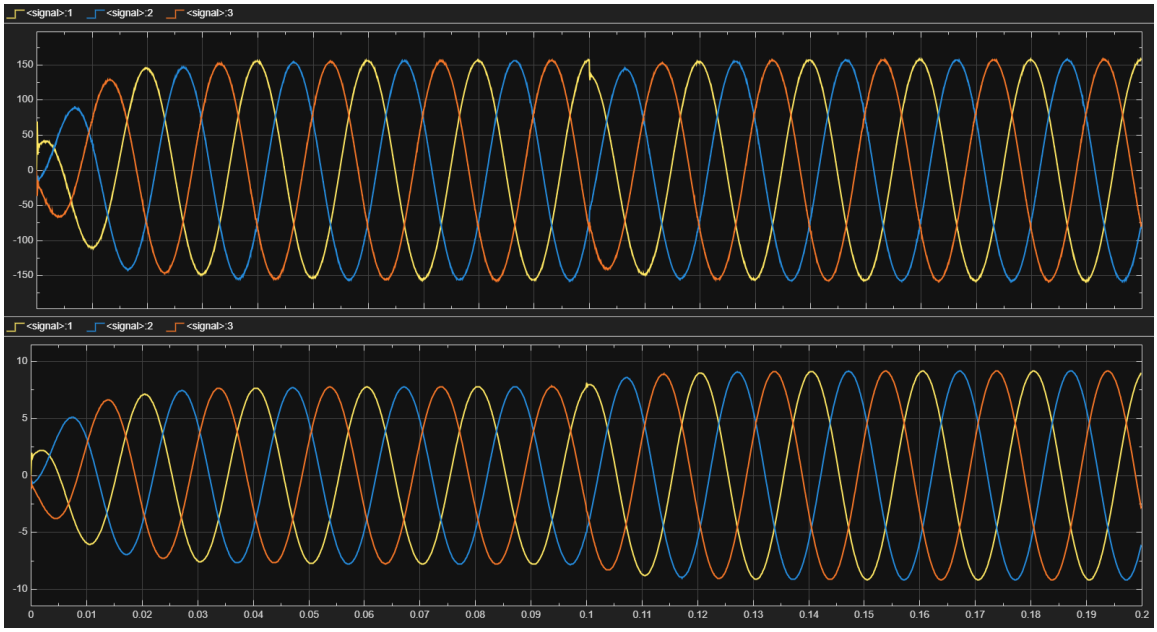

Figure 6: Voltage and current waveforms under Droop Control of inverter 1 in abc coordinates.

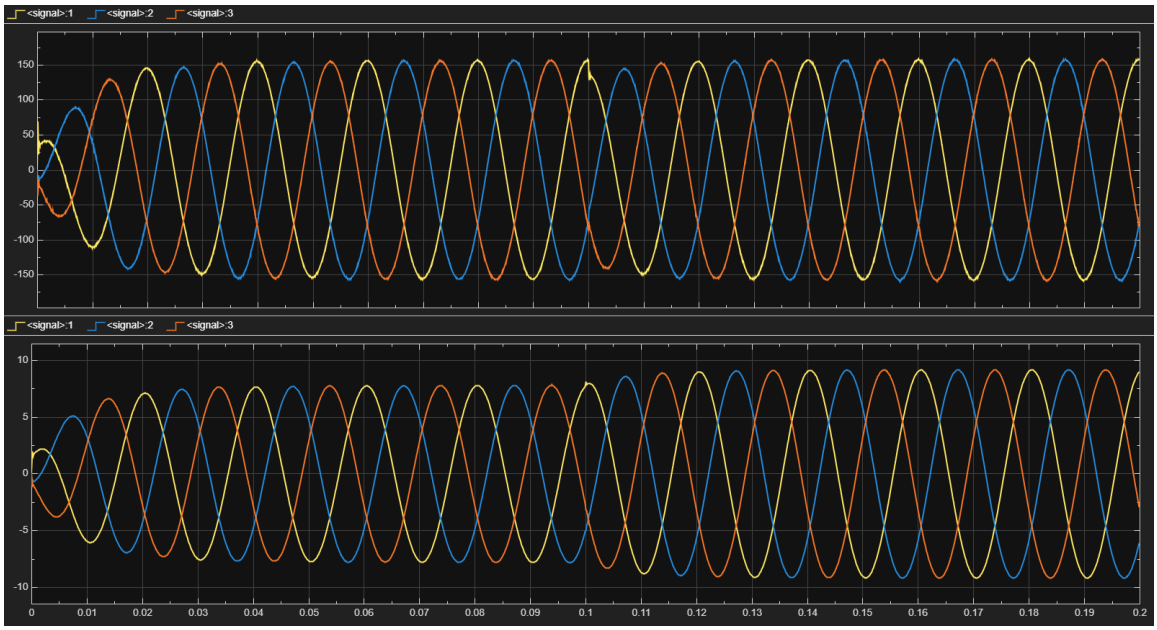

Figure 7: Voltage and current waveforms under Droop Control of inverter 2 in abc coordinates.

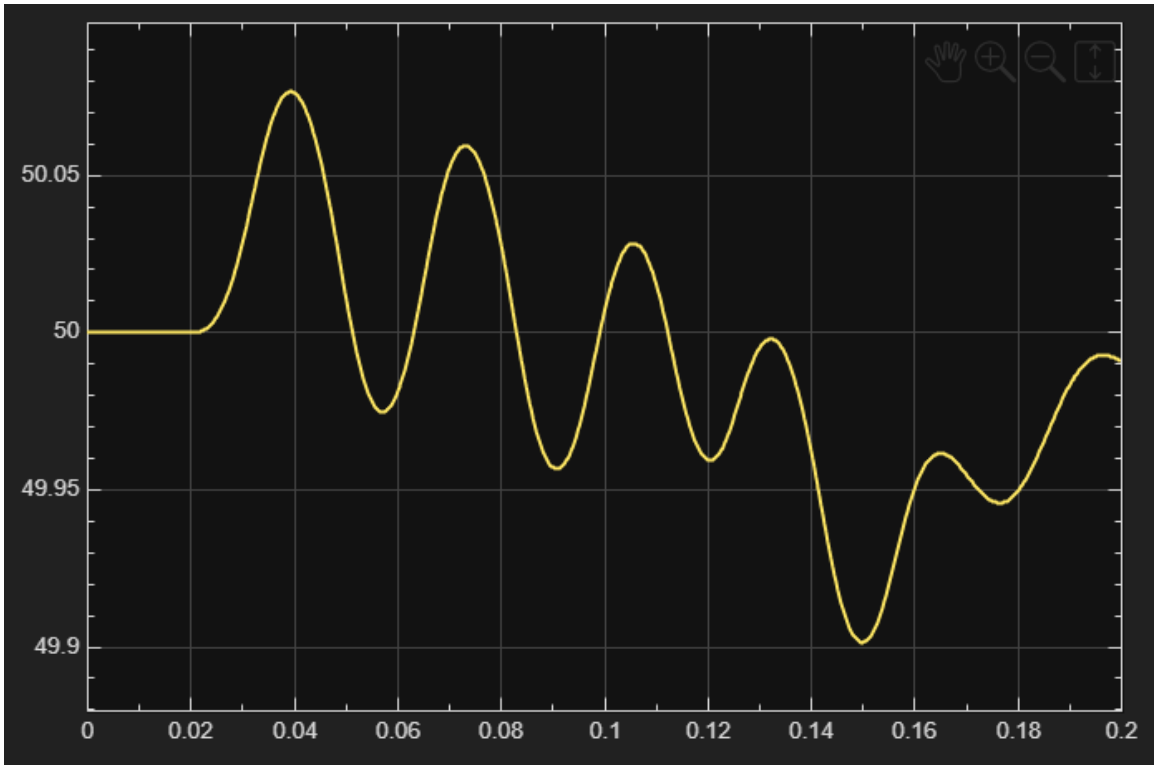

Figure 8: Frequency of Droop Control.

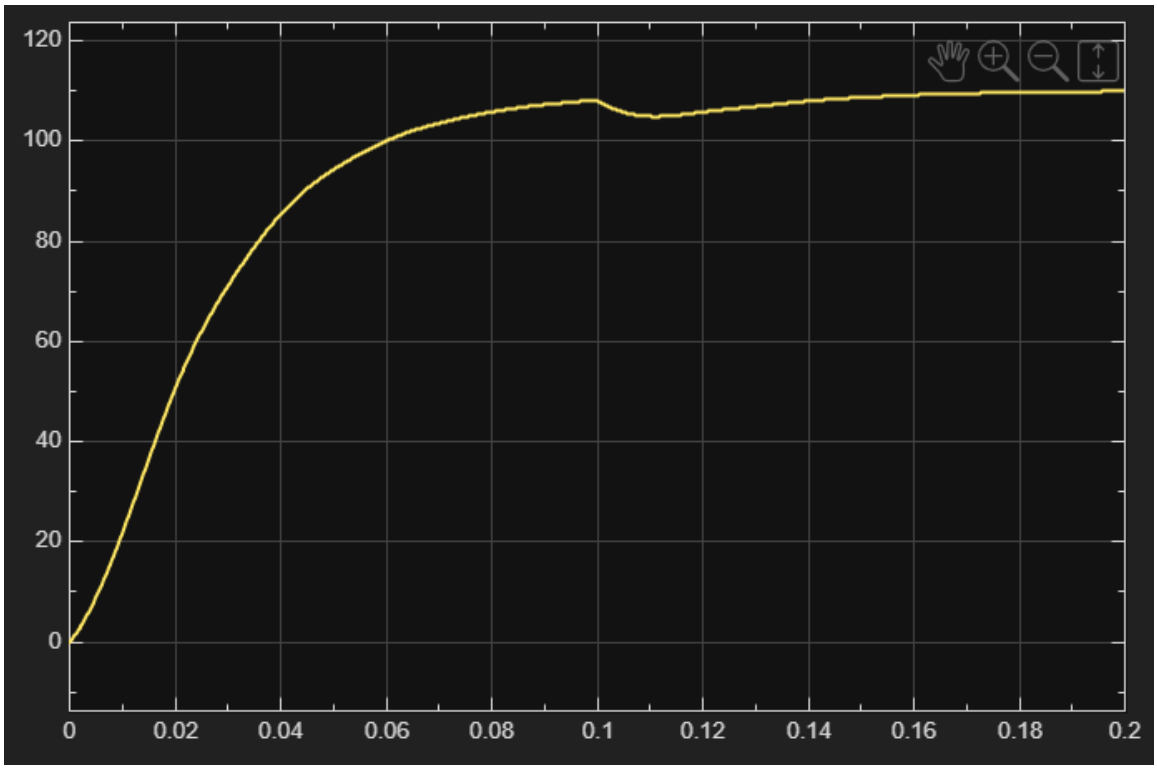

Figure 9: RMS voltage of Droop Control.

B.2 Virtual Synchronous Machine Results

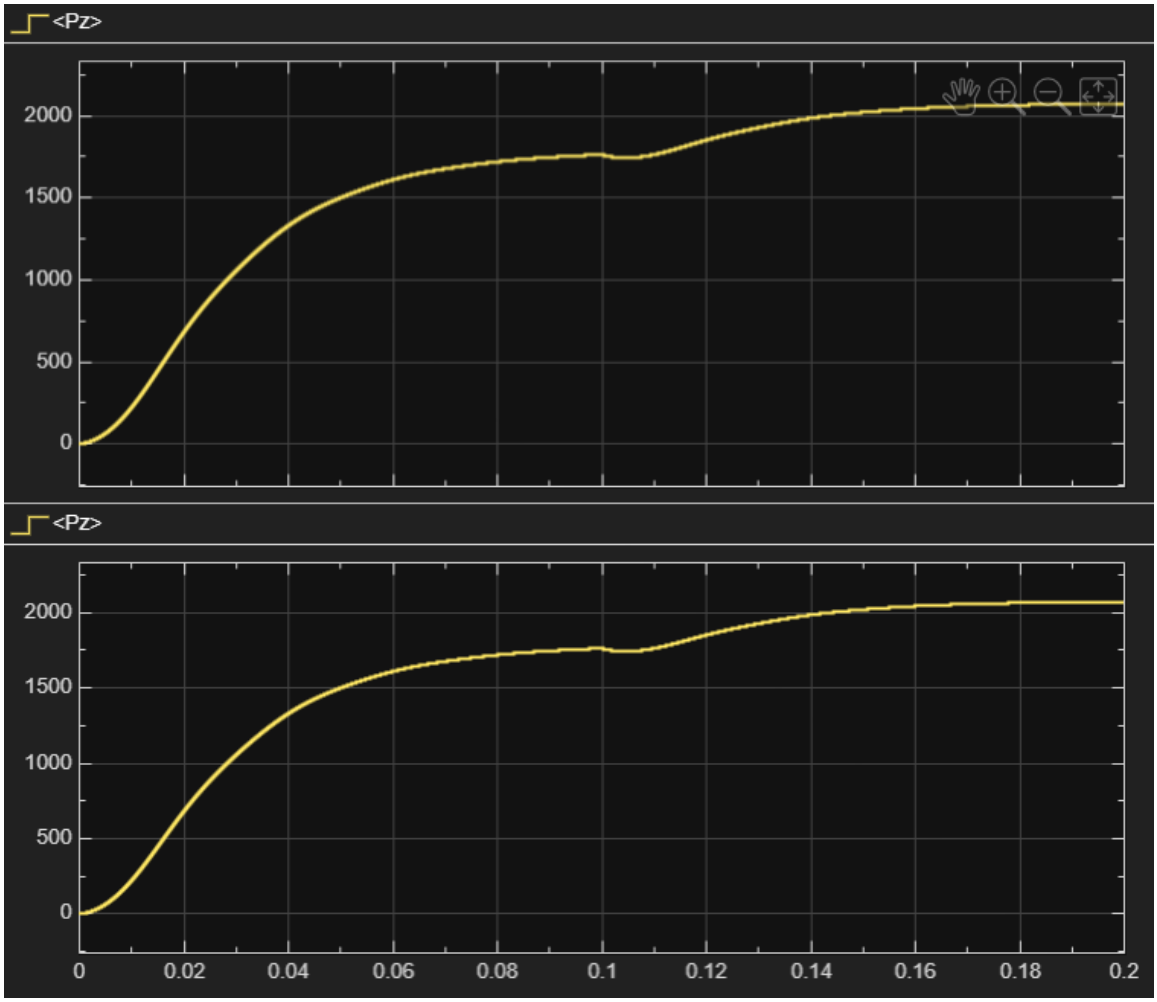

Figure 10: Active power response under VSM Control.

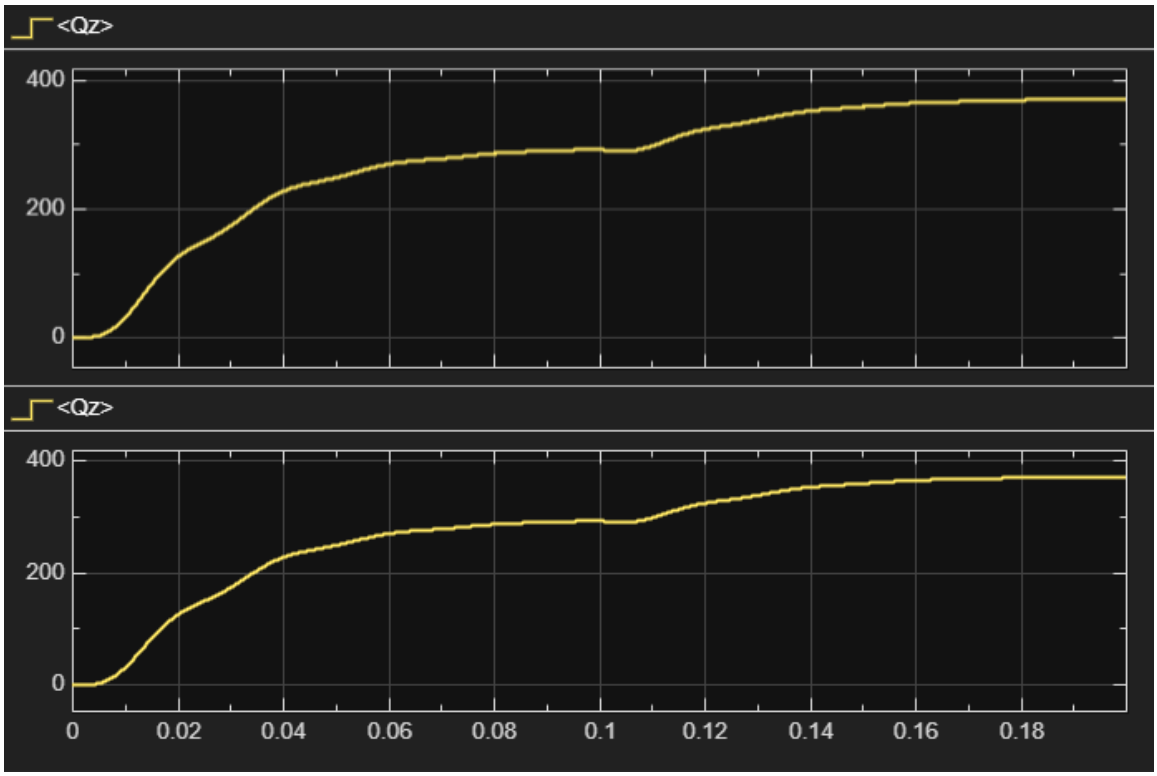

Figure 11: Reactive power response under VSM Control.

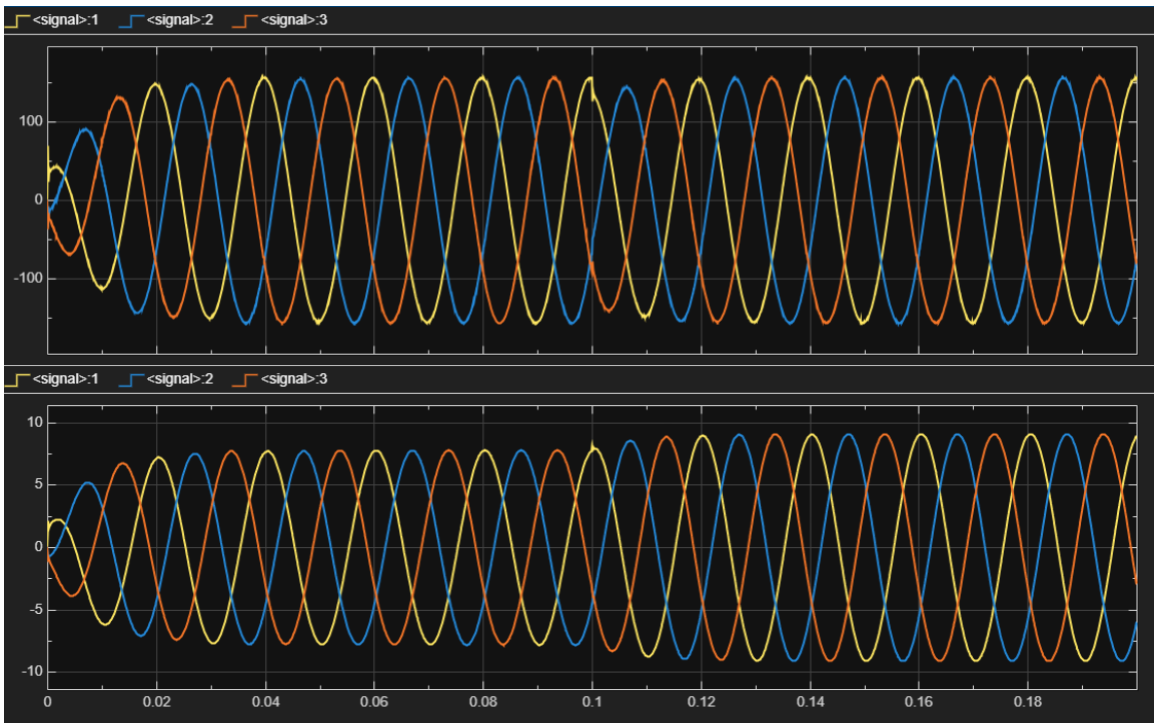

Figure 12: Voltage and current waveforms under VSM Control of inverter 1 in abc coordinates.

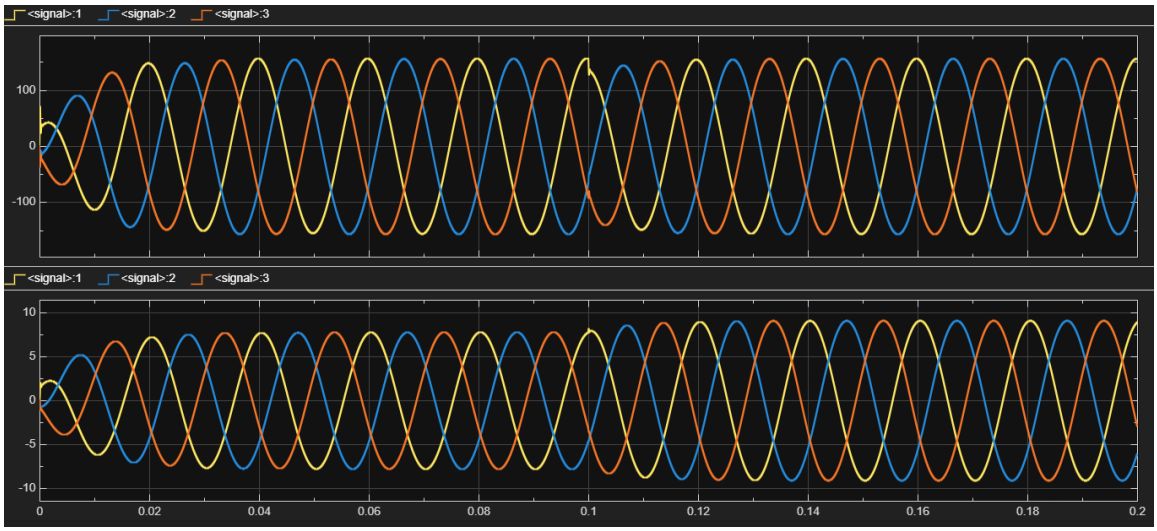

Figure 13: Voltage and current waveforms under VSM Control of inverter 2 in abc coordinates.

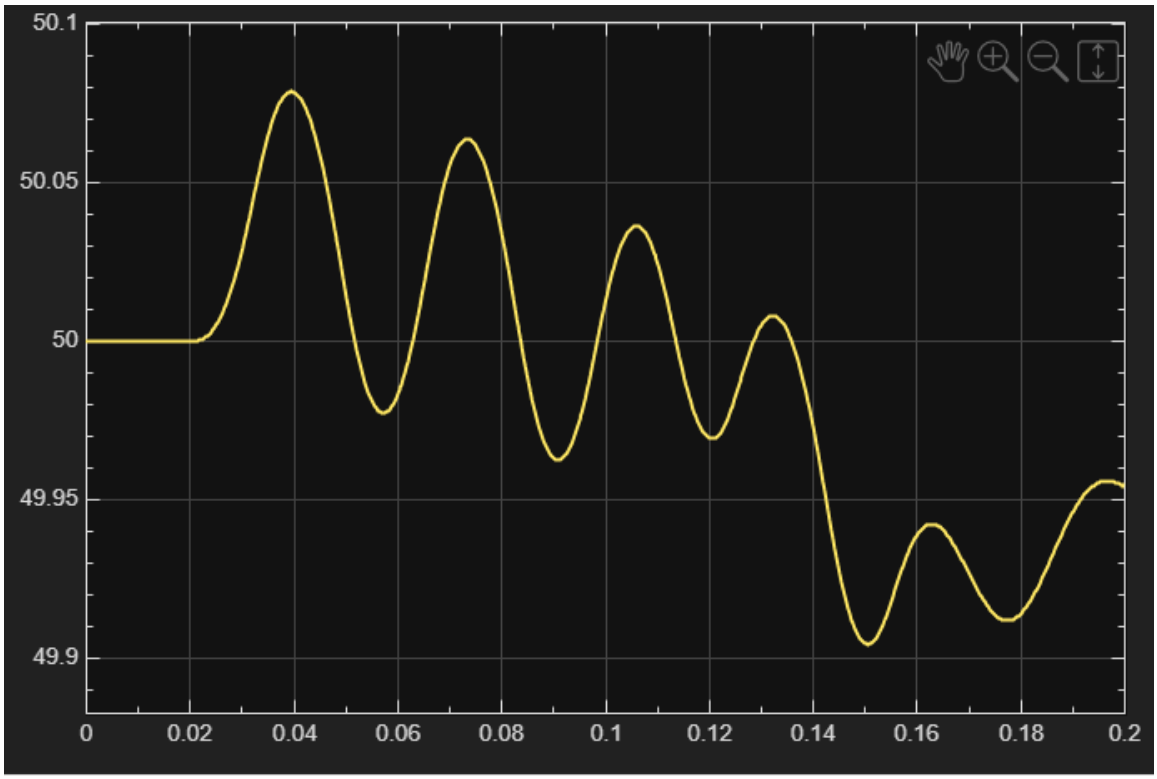

Figure 14: Frequency of VSM Control.

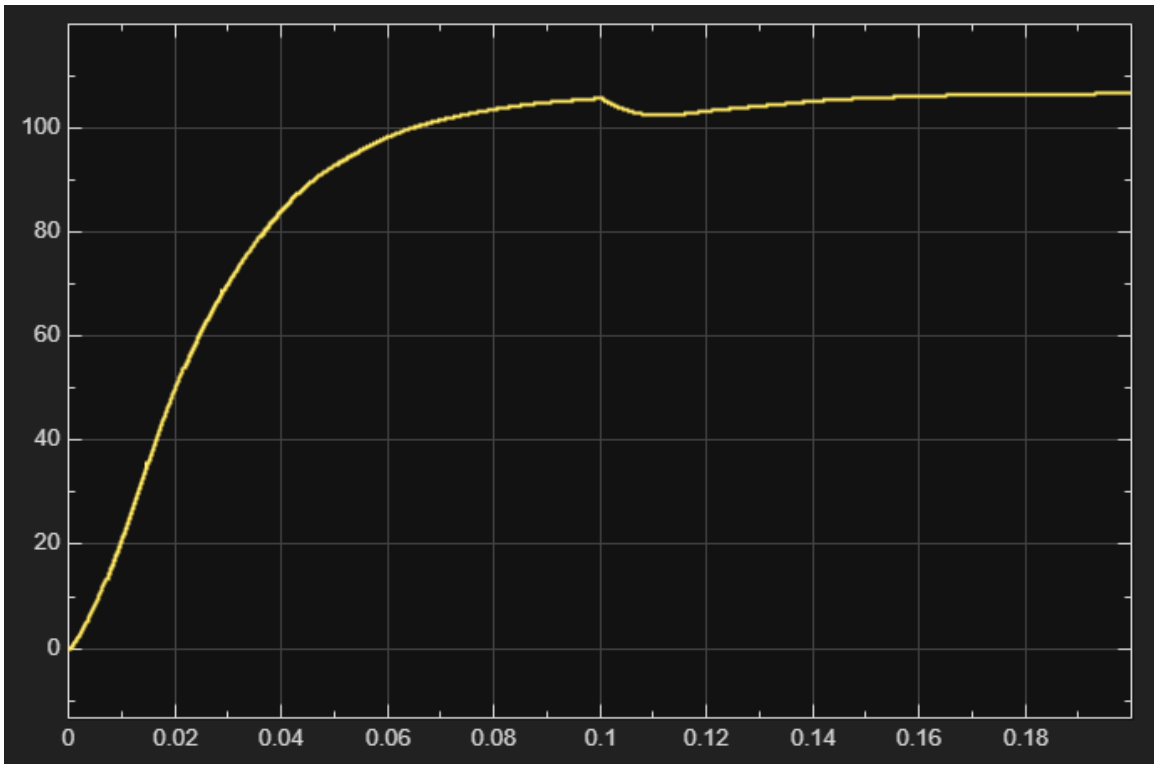

Figure 15: RMS voltage of VSM Control.

B.3 Matching Control Results

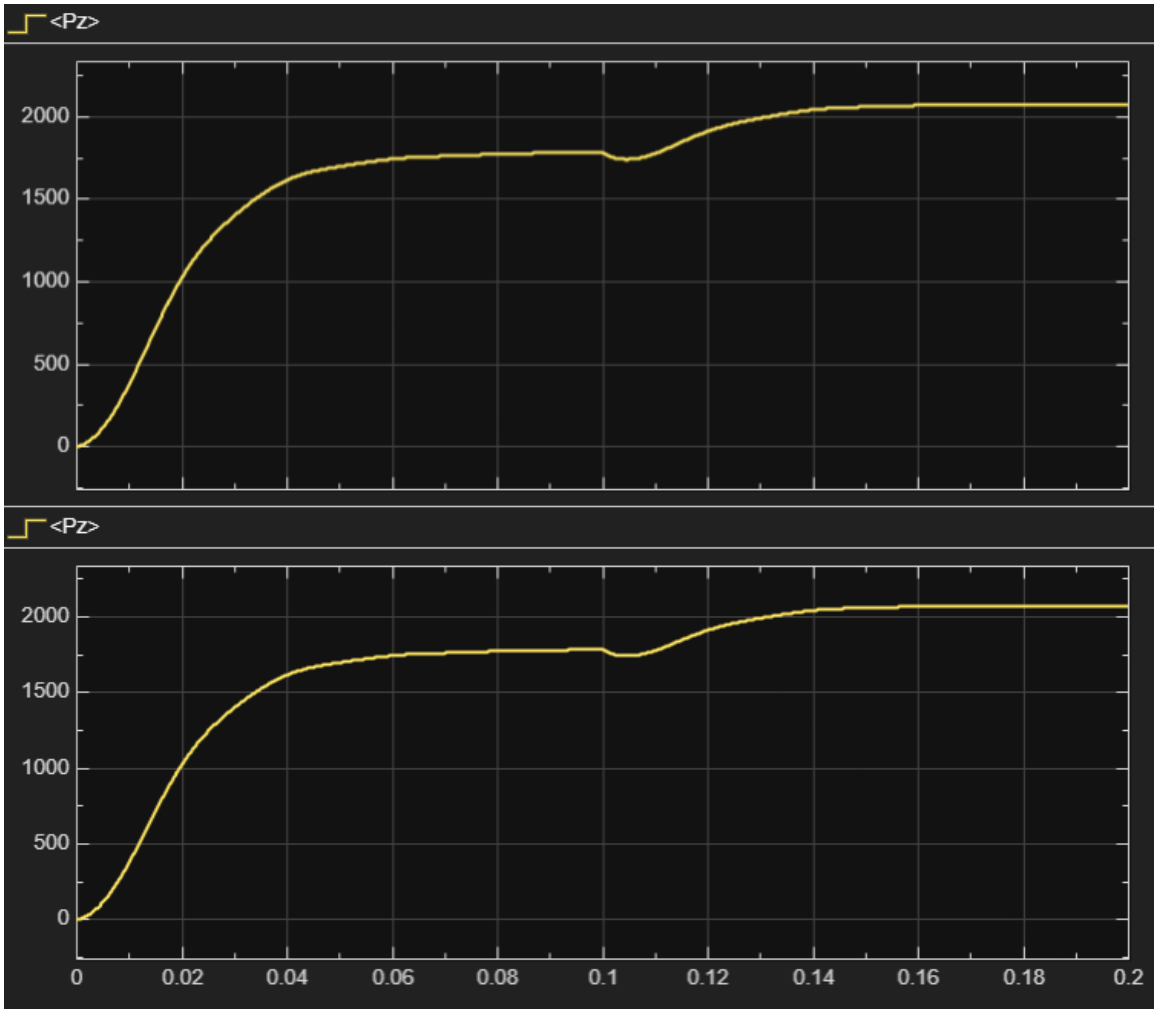

Figure 16: Active power response under Matching Control.

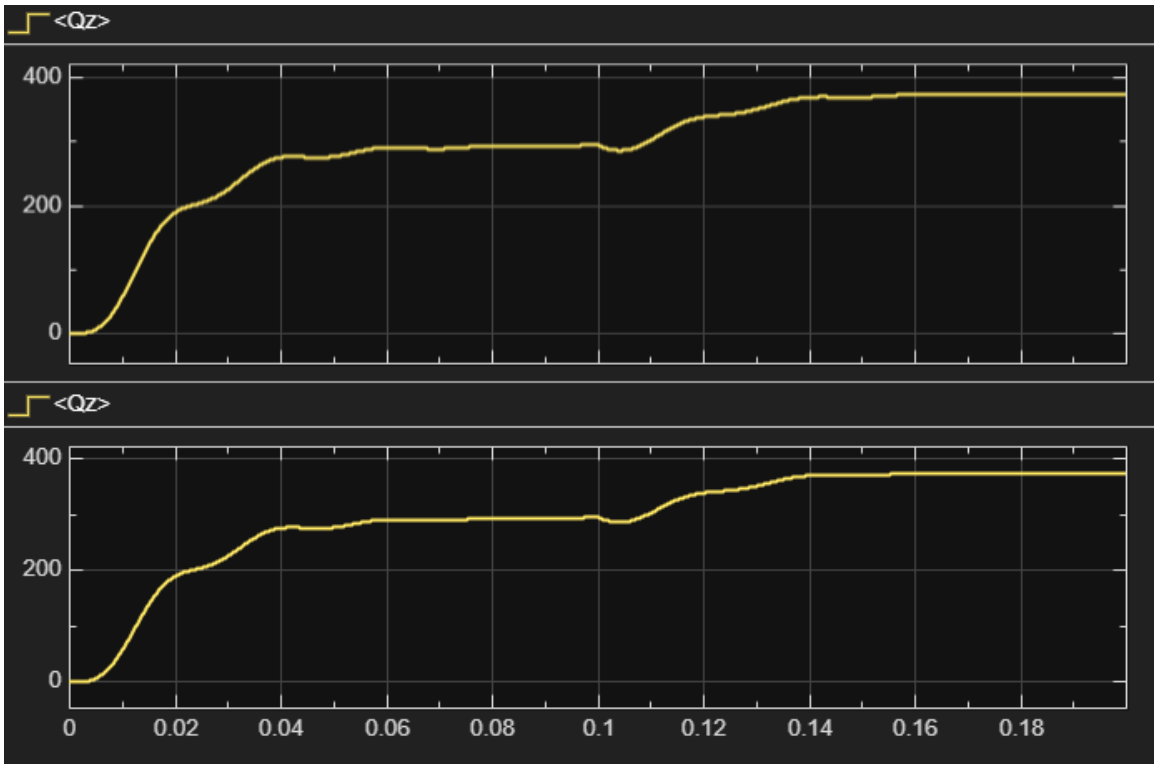

Figure 17: Reactive power response under Matching Control.

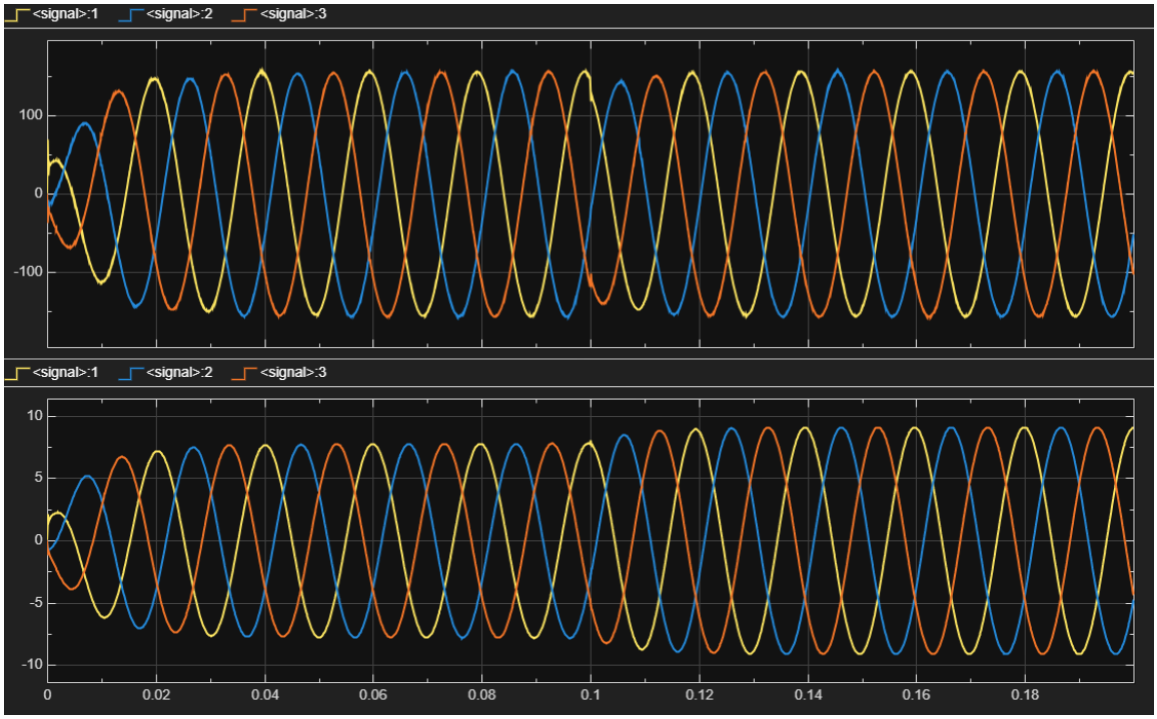

Figure 18: Voltage and current waveforms under Matching Control of inverter 1 in abc coordinates.

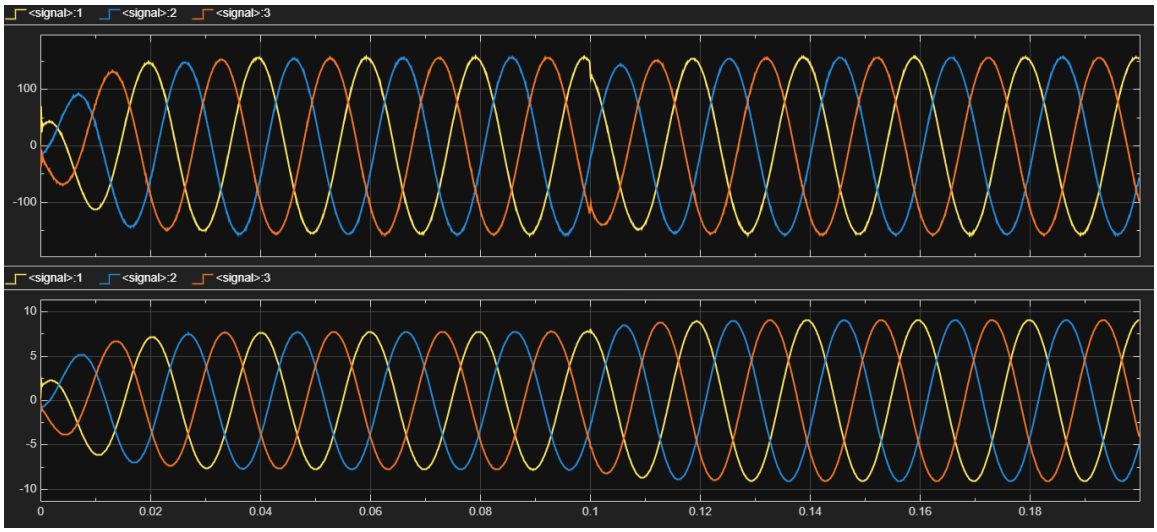

Figure 19: Voltage and current waveforms under Matching Control of inverter 2 in abc coordinates.

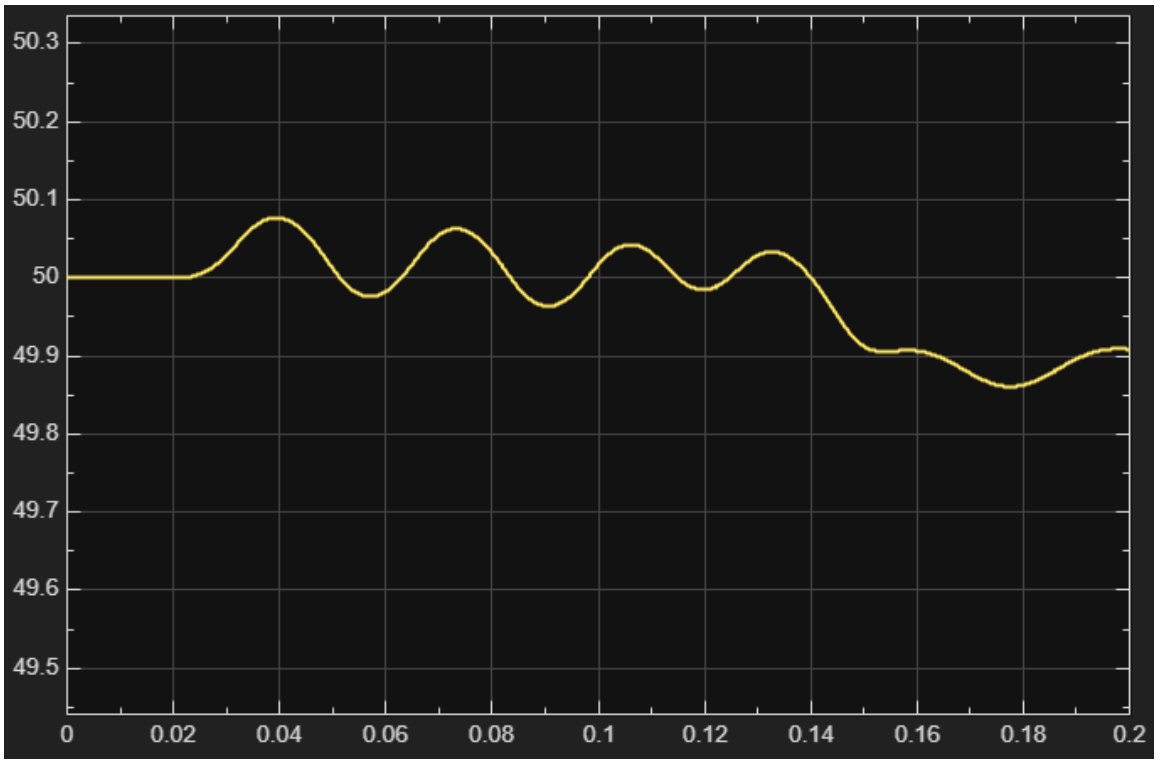

Figure 20: Frequency of Matching Control.

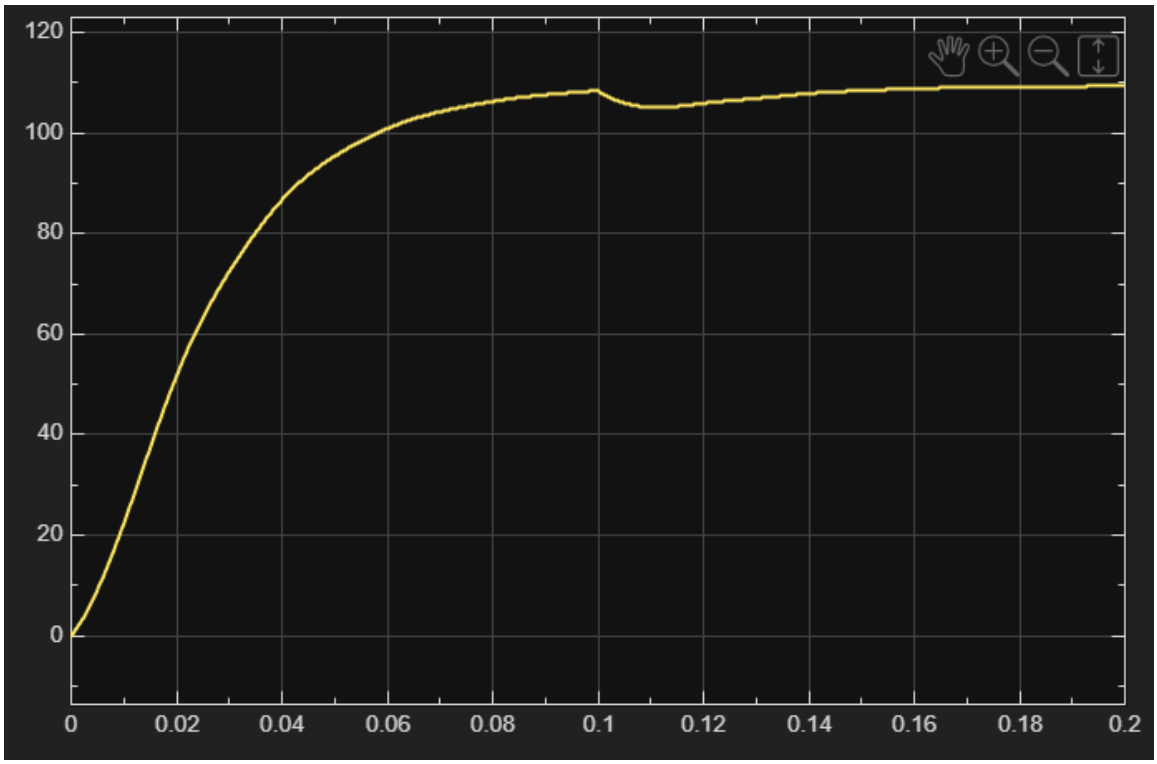

Figure 21: RMS voltage of Matching Control.